

# The geometry of blenders in a three-dimensional Hénon-like family

Stefanie Hittmeyer<sup>1</sup>, Bernd Krauskopf<sup>1</sup>, Hinke M Osinga<sup>1</sup>, Katsutoshi Shinohara<sup>2</sup>

<sup>1</sup> Department of Mathematics, The University of Auckland,  
Private Bag 92019, Auckland 1142, New Zealand

<sup>2</sup> Graduate School of Commerce and Management, Hitotsubashi University,  
2-1 Naka, Kunitachi, Tokyo 186-8601, Japan

November 2017

## Abstract

A blender is an intricate geometric structure of a diffeomorphism of dimension at least three. Its characterising feature is that its invariant manifolds behave as geometric objects of a dimension that is larger than expected from the dimensions of the manifolds themselves. We consider an explicit Hénon-like family of three-dimensional maps and show that it has a blender in a specific parameter regime. Advanced numerical techniques for the computation of one-dimensional stable and unstable manifolds enable us to present images of actual blenders and their associated manifolds. Moreover, these techniques allow us to present strong numerical evidence for the existence of the blender over a larger parameter range, as well as its disappearance beyond this range.

## 1 Introduction

In this paper we develop and employ an advanced numerical approach to investigate a three-dimensional diffeomorphism that exhibits an invariant object of complicated spatial structure called a *blender*. The stable manifold of a blender is so ‘dense’ that it acts geometrically as a set of higher dimension. The notion of a blender was introduced by Bonatti and Díaz in 1996 [5] to construct examples of an important class of higher-dimensional chaotic dynamical systems, called *robust non-uniformly hyperbolic* systems. Reference [8] is a very good entry point into the literature for this active area of research.

The construction in [5] is an abstract example of a diffeomorphism of dimension at least three. The authors give a sufficient condition for the existence of a blender, which shows how the blender property emanates from the construction in an indirect fashion. In the recent introductory article of Bonatti, Crovisier, Díaz and Wilkinson [4], they demonstrate how the conditions assumed in [5] generate a blender by constructing an affine-model blender; see also [8]. More specifically, a *horseshoe* is generated by the iterated stretching and folding of suitable rectangles in two dimensions [28]. The authors of [4] generalize this construction to three dimensions by adding a certain weak expansion and translation in the third variable, which effectively leads to iterated stretching and folding of suitable rectangular boxes. While this geometric construction of a blender is more intuitive and easier to understand, the constructed map is a toy model. In this paper, we address the natural question what a blender and its stable manifold look like in an explicitly defined map.

We study the family of polynomial diffeomorphisms

$$H(x, y, z) = (y, \mu + y^2 + \beta x, \xi z + y). \tag{1}$$

It reduces in the first two coordinates  $x$  and  $y$  to the planar diffeomorphism

$$h(x, y) = (y, \mu + y^2 + \beta x), \quad (2)$$

which is conjugate to the Hénon map [15]. The third coordinate of (1) is a shear in the  $z$ -coordinate, for which the strength of attraction or repulsion is determined by the parameter  $\xi$  (which is the respective eigenvalue).

The Hénon-like family  $H$  of (1) is a good candidate for a concrete system with a blender, because it is a perturbation of the family of endomorphisms

$$F(x, y, z) = (y, \mu + y^2 + \kappa z^2, \xi z + y), \quad (3)$$

constructed by Díaz, Kiriki and Shinohara in [11]. These authors showed that (3) has a blender for  $\mu \in (-10, -9)$ ,  $\xi \in (1.18, 1.19)$  and  $\kappa \in (0, 10^{-4})$ . In (1) we introduced the term  $\beta x$  to make the map  $H$  invertible. Moreover, we eliminated the term  $\kappa z^2$ , since the parameter  $\kappa \in (0, 10^{-4})$  is very small. In this way, the first two variables in (1) are independent of the third variable, yielding the overall structure of the planar Hénon-like map extended by a shear. Due to the robustness of the blender in (3), we expect to find a blender also in the perturbed map (1) for similar ranges of  $\mu$  and  $\xi$ , and for sufficiently small  $\beta$ . In what follows, we fix  $\mu = -9.5$  and  $\beta = 0.1$ , which is a parameter point for which the planar Hénon map  $h$  has a full horseshoe. In line with the theory and the results of [11], a blender should exist for a sufficiently weak, central unstable direction, that is, for  $\xi > 1$  sufficiently close to 1.

In this paper we employ advanced numerical methods for the computation of one-dimensional stable and unstable manifolds of a saddle fixed point of the family  $H$  as very long parametrized curves. This allows us to produce the first images of the manifold structure of a blender. An important ingredient of this approach is the compactification of the parameter space  $\mathbb{R}^3$  of (1) to a bounded cylinder. This facilitates a much more efficient computation of the manifolds, as well as their representation in their entirety.

We check for and illustrate a particular geometric property to identify a blender of  $H$ , which we refer to as the *carpet property*: the closure of a suitable projection of the one-dimensional (un)stable manifold fills a two-dimensional region. More precisely, we observe that, for  $\xi = 1.185$ , the computed part of the one-dimensional stable manifold becomes more and more dense in projection onto the  $(x, z)$ -plane when it is computed for increasingly larger arclength. Hence, we conclude that there is a blender of  $H$  for this parameter point; see already figure 3. On the other hand, for sufficiently large  $\xi > 1$ , we find that the same projection of the stable manifold has a Cantor-set structure with obvious gaps, which do not disappear when the manifold is computed up to larger arclength. We conclude that the manifold no longer has the carpet property and, hence, that the map  $H$  no longer admits a blender; see already figures 8 and 9.

We quantify these findings by constructing a numerical test to check for the carpet property. Namely, we define and determine the *maximal gap* between the projected segments of the computed part of the one-dimensional stable manifold up to a given arclength. We then check whether the maximal gap converges to zero or stays at some positive value when the arclength is doubled repeatedly. We also compute the maximal gap as a function of the projection angle to check for the robustness of the carpet property. This computational approach allows us to show that the blender exists for quite a large parameter regime, well beyond the suggested value of  $\xi = 1.185$  and up to a parameter value  $\xi^* \approx 1.843$ , at which the carpet property is lost and the hyperbolic set ceases to be a blender. The approximation of the stable manifold and the associated maximal gap to verify the carpet property become computationally more expensive as  $\xi > 1$  approaches  $\xi = 1$ ; this is because  $\xi$  is one of the eigenvalues of the saddle fixed point, which is no longer hyperbolic for  $\xi = 1$ .

We conclude that  $H$  has a blender for  $1 < \xi < \xi^*$ , which includes the parameter point  $\mu = -9.5$ ,  $\xi = 1.185$  and  $\beta = 0.1$  suggested by the work in [11]. This insight motivated us to prove that  $H$  indeed has a blender at this parameter point, by adapting the proof from the endomorphism  $F$  to the diffeomorphism  $H$ . The proof is very complimentary in spirit to the computation of invariant manifolds. It requires one to show how a certain box in phase space maps back to itself, which involves checking a number of technical conditions; the proof can be found in Appendix A.

For  $\xi < 1$  the fixed point admits a two-dimensional stable and a one-dimensional unstable manifold. Hence, we can also apply our approach to investigate the properties of the one-dimensional unstable manifold of the map (1) for  $\xi < 1$ , given as the one-dimensional stable manifold of the inverse of (1). We find that this unstable manifold also has the carpet property for  $\xi < 1$  near  $\xi = 1$  when projected onto the  $(y, z)$ -plane; see already figures 12 and 13. Indeed, the maximal gap converges to zero in this case. We also find that the maximal gap converges to a positive value, and the carpet property is lost, when  $\xi < 1$  is decreased too much; more specifically for  $\xi < \xi^{**} \approx 0.515$  the hyperbolic set of  $H$  is no longer a blender.

Overall, we demonstrate that our numerical approach is able to check whether the carpet property is satisfied or not and, hence, whether the Hénon-like map  $H$  has a blender or not. In this way, we are able to identify the parameter region of existence of a blender. Moreover, our results suggest that there are bifurcations of the hyperbolic set that corresponds to the disappearance or creation of a blender. These results should be viewed as motivation for future development of theory and novel methods of proof. Indeed, we believe that the numerical methods presented here will be of use also in related situations. As an initial example and outlook, we present an observation for the classical parameter regime of the Hénon map (2), namely, for fixed  $\mu = -1.4$  and  $\beta = 0.3$ . Then, for  $\xi < 1$  near  $\xi = 1$ , the map  $H$  has a chaotic attractor that is the closure of the unstable manifold of a saddle fixed point, which has the carpet property. We refer to this object as a blender-like attractor; see already figure 19. Its study is ongoing and will be reported elsewhere.

This paper is organized as follows. In section 2, we introduce the necessary background and notation. More specifically, in section 2.1, we give the definitions of a blender and of non-uniform hyperbolicity, and briefly review relevant examples from the literature. We then introduce, in section 2.2, the properties of the map  $H$ , introduce the compactification of the phase space and relate the phase space of the planar Hénon map  $h$  with that of the family  $H$ . In section 3, we investigate the stable manifold of the saddle fixed point for  $\xi = 1.185, 1.6, 2$ , and  $2.5$ . In section 3.2, we introduce the computation of the *maximal gap* as a numerical method for the detection of the carpet property. Section 4 is dedicated to the one-dimensional unstable manifold of the saddle fixed point for  $\xi = 0.9, 0.7, 0.5$  and  $0.3$ , including the computation of the maximal gap for these values of  $\xi < 1$ . We end, in section 5, with conclusions and directions for future work. As an outlook we present, in section 5.1, our observation of a blender-like attractor of  $H$  for the classical Hénon parameter regime. Appendix A contains further information about our computations of one-dimensional global manifolds, and Appendix A contains the proof of existence of the blender of  $H$  for  $\mu = -9.5$ ,  $\xi = 1.185$  and  $\beta = 0.1$ .

## 2 Background and Notation

We now introduce the necessary definitions and review some examples of non-uniformly hyperbolic systems in section 2.1; we introduce the properties of the maps (1) and (2), the compactification of the phase space and the invariant manifolds in sections 2.2–2.4; and we define the carpet property in section 2.5.

## 2.1 Definitions and examples in the literature

For the following definitions and as an entry point to the literature, see [8]. We start our discussion with the central concept of a *hyperbolic set* of a diffeomorphism, which is an invariant set such that its tangent bundle can be decomposed continuously into stable and unstable subspaces that are invariant under the derivative. In particular, a hyperbolic set admits *stable and unstable manifolds* given as the sets of points that converge to the hyperbolic set under forward and backward iteration of the diffeomorphism, respectively. The dimensions of the stable and unstable subspaces are called the *stable* and *unstable indices* of the hyperbolic set, respectively. Hyperbolic saddle fixed points and periodic points are trivial examples of hyperbolic sets. The *nonwandering set*  $\Lambda$  of a diffeomorphism consists of points with the property that each of their neighbourhoods contains a point that returns to this neighbourhood after a finite number of iterations. The set  $\Lambda$  contains the fixed points, the periodic points, the homoclinic points, and the  $\omega$ - and  $\alpha$ -limit sets (the accumulation points under forward and backward iteration, respectively). It is said to be *transitive* if  $\Lambda$  contains a dense orbit. In particular, a transitive nonwandering set cannot be split into smaller closed invariant subsets. A diffeomorphism is called *uniformly hyperbolic* or *Axiom A* if the nonwandering set  $\Lambda$  is a hyperbolic set and the set of periodic points is dense in it. Existing theory gives a good understanding of the structure and structural stability of uniformly hyperbolic systems and their hyperbolic sets; we refer again to [8].

While there are many examples of Axiom-A diffeomorphisms, it is not easy to construct examples of diffeomorphisms that robustly fail to be uniformly hyperbolic. By this we mean diffeomorphisms that admit a  $C^r$ -open neighbourhood of non-uniformly hyperbolic diffeomorphisms for some  $r \geq 1$ . Two mechanisms that generate robust non-uniform hyperbolicity in a diffeomorphism are robust heterodimensional cycles and robust homoclinic tangencies. It is expected that these two phenomena are closely related; the exact nature of their relationship is an active area of research [8]. We now introduce these two concepts in detail and discuss some examples.

Two hyperbolic sets are connected by a *heteroclinic cycle* if the stable manifold of the one hyperbolic set intersects the unstable manifold of the other, and vice versa. A *heterodimensional cycle* is a heteroclinic cycle between two hyperbolic sets of different stable indices. This means that heterodimensional cycles can only occur in diffeomorphisms of dimension at least three. The simplest example is a heterodimensional cycle in a three-dimensional diffeomorphism between two fixed points with stable manifolds of dimensions one and two, respectively. By definition, a system with a heterodimensional cycle is non-uniformly hyperbolic since the fixed points are nonwandering and their indices are different, meaning that the associated nonwandering set cannot have a uniform splitting into stable and unstable directions. A heterodimensional cycle is called  *$C^r$ -robust* for  $r \geq 1$  if every ( $C^r$ -)close diffeomorphism admits a heterodimensional cycle.

In 1996, Bonatti and Díaz introduced the notion of a blender [5], which can be used to construct examples of robust heterodimensional cycles. They subsequently gave a more general definition in [7], which we use here. A transitive hyperbolic set  $\Lambda$  of unstable index  $k \geq 2$  is called a *blender* if there is a  $C^1$ -open set of embeddings of  $(k - 1)$ -dimensional disks into the  $n$ -dimensional phase space that each intersect the local stable manifold of the hyperbolic set. Moreover, this property is robust in the sense that it also holds for the corresponding hyperbolic set of every sufficiently  $C^1$ -close diffeomorphism. Colloquially, this means that the stable manifold acts as if it were of dimension  $n - k + 1$ , instead of  $n - k$ .

The phenomena of blenders and heterodimensional cycles are closely related. For example, a blender can naturally emerge after the bifurcation of a heterodimensional cycle [7]. More precisely, a heterodimensional cycle gives rise to nearby saddle-node bifurcations. Some of

these bifurcations admit so-called *strong homoclinic intersections*; these are special configurations of invariant manifolds of the periodic orbits involved. Together, these saddle-node bifurcations and strong homoclinic intersections generate a blender. On the other hand, a blender of unstable index  $k \geq 2$  can be used to construct robust heterodimensional cycles in a diffeomorphism of dimension  $n \geq 3$ . Indeed, the blender can provide the robust intersection of its  $(n - k)$ -dimensional stable manifold with the  $(k - 1)$ -dimensional unstable manifold of another hyperbolic set. Note that the  $k$ -dimensional unstable manifold of the blender generically intersects the  $(n - k + 1)$ -dimensional stable manifold of the other hyperbolic set.

The other mechanism that generates robust non-uniform hyperbolicity are robust homoclinic tangencies. A hyperbolic set has a *homoclinic tangency* if it admits a nontransversal intersection between its stable and unstable manifolds. A system with a homoclinic tangency is non-uniformly hyperbolic because the point of tangency is nonwandering, but its tangent bundle cannot be decomposed into stable and unstable subspaces. A homoclinic tangency is  $(C^r)$ -robust and the associated hyperbolic set is called  $(C^r)$ -wild if the corresponding hyperbolic set of every  $C^r$ -close diffeomorphism admits a homoclinic tangency for  $r \geq 1$ . Robust homoclinic tangencies imply robust non-uniform hyperbolicity and we refer to the occurrence of a wild hyperbolic set as *wild chaos*.

The first example of  $C^2$ -robust homoclinic tangencies was constructed by Newhouse in the late sixties [25]. He presented a two-dimensional diffeomorphism with homoclinic tangencies that persist under  $C^2$ -perturbations, but the arguments cannot be extended to the  $C^1$ -topology [32, 24]. The construction is local, in the sense that it involves only the information about the existence of tangencies and their “thickness,” which represents (fractal-)geometric information about the invariant manifold.

In 2006, Bamón, Kiwi and Rivera-Letelier constructed an explicit two-dimensional endomorphism occurring as the reduction of a wild Lorenz-like attractor in a vector field of dimension at least five [2]; see also [30, 31] for a similar construction. These attractors are *Lorenz-like* in the sense that they are generalizations of the famous Lorenz attractor to higher dimensions [22]. The authors of [2] use a construction similar to a blender, which they refer to as a “solenoidal blender.” In [16, 17], a specific sequence of bifurcations was identified that generates wild chaos in this system and governs the transition from an expanding to a contracting Lorenz-like attractor.

Two abstract examples of three-dimensional diffeomorphisms with wild chaos and blenders are constructed in [29] and in [6]. An explicit example of a Hénon-like diffeomorphism with a discrete wild Lorenz-like attractor is investigated theoretically and numerically in [13, 14]. This diffeomorphism is Hénon-like in the sense that it is a three-dimensional generalization of the Hénon map (2).

Finally, the only known explicit example of a vector field with a heterodimensional cycle is a four-dimensional vector field model of intracellular calcium dynamics. It was studied in [33], where it was shown with advanced numerical techniques, based on two-point boundary-value problem formulations, that there is indeed a heterodimensional cycle between two periodic orbits of different indices. The heterodimensional cycle was found and continued as a curve in two system parameters. It is presently under investigation whether there are nearby and robust heterodimensional cycles or even blenders. Specifically, in [23] the properties of invariant manifolds of periodic orbits in this system are investigated numerically by examining intersections with a three-dimensional Poincaré section.

A four-dimensional vector field is also considered in [21], where it is shown that a heterodimensional cycle between two periodic orbits is created by a saddle-focus equilibrium with a pair of homoclinic loops. These authors give a sufficient condition that guarantees the existence of heterodimensional cycles in vector fields after a perturbation. While it is not difficult to verify that suitable vector fields must exist, we do not know if there is an explicitly defined (such as,

polynomial) vector field satisfying this condition.

## 2.2 Basic properties of the map $H$

The Hénon map (2) is classically studied for the parameter values  $\mu = -1.4$  and  $\beta = 0.3$ , where it admits the well-known chaotic Hénon attractor [3]. In Sections 3 and 4 we investigate the map (1) in a different parameter regime, namely, for  $\mu = -9.5$  and  $\beta = 0.1$ . For these parameter values the Hénon map (2) features a *full horseshoe*, that is, the nonwandering set  $\Lambda_h$  of (2) is topologically conjugate to the full shift on two symbols [10]. The blender of the map (1) is the lift of the hyperbolic set  $\Lambda_h$  to a hyperbolic set  $\Lambda$  of (1).

In the parameter regimes we consider in this paper, the Hénon map (2) has two saddle fixed points  $p_h^+ := (\rho_h^+, \rho_h^+)$  with  $\rho_h^+ > 0$  and  $p_h^- := (\rho_h^-, \rho_h^-)$  with  $\rho_h^- < 0$ . These lift to the two saddle fixed points  $p^+$  and  $p^-$  of three-dimensional map  $H$ , given by

$$p^\pm := \left( \rho_h^\pm, \rho_h^\pm, \frac{\rho_h^\pm}{1-\xi} \right).$$

Their eigenvalues are the two eigenvalues of  $p_h^\pm$  of (2) and  $\xi$ .

For  $\mu = -9.5$  and  $\beta = 0.1$ , we have

$$p^+ \approx \left( 3.565, 3.565, \frac{3.565}{1-\xi} \right)$$

with eigenvalues approximately  $-0.014$ ,  $7.1438$  and  $\xi$ , and

$$p^- \approx \left( -2.665, -2.665, \frac{-2.665}{1-\xi} \right)$$

with eigenvalues approximately  $0.0187$ ,  $-5.3485$  and  $\xi$ . For  $\xi = 1.185$ , the corresponding eigenvectors of  $p^+$  are approximately  $(0.9998, -0.014, 0.0117)$ ,  $(0.1368, 0.9769, 0.1640)$  and  $(0, 0, 1)$ , and those of  $p^-$  are approximately  $(-0.9997, -0.0187, 0.0160)$ ,  $(0.1817, -0.9720, 0.1488)$  and  $(0, 0, 1)$ . Note that the strong stable eigenspaces of  $p^\pm$  are nearly parallel to the  $x$ -axis, the strong unstable eigenspaces are nearly parallel to the  $y$ -axis, and the central or weak unstable eigenspace is simply the  $z$ -axis.

## 2.3 Compactification of phase space

In order to obtain a global picture of the dynamics and to aid the computation of global invariant manifolds, we compactify the phase space  $\mathbb{R}^3$ . We choose a form of compactification that reflects the structure of the map (1). More specifically, we compactify the  $(x, y)$ -plane of (2) to the Poincaré disk  $\mathcal{D} := \{(\bar{x}, \bar{y}) \mid \|(\bar{x}, \bar{y})\| \leq 1\}$  and the  $z$ -axis of the shear to the interval  $\mathcal{I} := \{(\bar{z}) \mid |\bar{z}| \leq 1\}$ , both by stereographic projection. Overall, this results in the compactification of the phase space  $\mathbb{R}^3$  of (1) to the cylinder

$$\mathcal{C} := \mathcal{D} \times \mathcal{I} = \{(\bar{x}, \bar{y}, \bar{z}) \mid \|(\bar{x}, \bar{y})\| \leq 1 \text{ and } |\bar{z}| \leq 1\}$$

by the transformation

$$T : \mathbb{R}^3 \rightarrow \mathcal{C} \tag{4}$$

$$(x, y, z) \mapsto (\bar{x}, \bar{y}, \bar{z}) := \left( \frac{x}{1+\|(x,y)\|}, \frac{y}{1+\|(x,y)\|}, \frac{z}{1+|z|} \right), \tag{5}$$

where  $\|(\cdot, \cdot)\|$  denotes the Euclidean norm. The boundary  $\partial\mathcal{C}$  of  $\mathcal{C}$  corresponds to infinity in the original coordinates.

The map  $H$  acts on (the interior of) the compactified phase space  $\mathcal{C}$  by conjugation with  $T$ , that is, as the conjugate map  $T \circ H \circ T^{-1}$ . For simplicity, we refer to this compactified map on  $\mathcal{C}$  also as  $H$ ; similarly, we denote the compactified fixed points  $T(p^\pm)$  also as  $p^\pm$ . The boundary  $\partial\mathcal{D}$  of the Poincaré disk corresponds to directions of escape to infinity of the (compactified) Hénon map (2). Its extension to  $\partial\mathcal{D}$  admits a sink  $q_h := (0, 1)$  and a source  $s_h := (-1, 0)$  on  $\partial\mathcal{D}$ . One can extend  $H$  to  $\partial\mathcal{C}$  in such a way that the points  $q^\pm := (0, 1, \pm 1)$  act as sinks and the points  $s^\pm := (-1, 0, \pm 1)$  act as sources on  $\partial\mathcal{C}$ . We work in the compactified phase space  $\mathcal{C}$  from now on.

## 2.4 Global manifolds

Let  $p$  be a hyperbolic saddle fixed point of a diffeomorphism  $f$  with a phase space  $M$  of dimension at least two. In a small neighbourhood  $V$  of  $p$ , the *local stable manifold* is defined as

$$W_{\text{loc}}^s(p) := \{v \in M \mid f^n(v) \in V \text{ for all } n \geq 0\}.$$

It is tangent to the stable eigenspace at  $p$  and can be globalized under backward images to obtain the *stable manifold*

$$W^s(p) := \bigcup_{n \geq 0} f^{-n}(W_{\text{loc}}^s(p)). \quad (6)$$

Similarly, the *local unstable manifold*

$$W_{\text{loc}}^u(p) := \{v \in M \mid f^{-n}(v) \in V \text{ for all } n \geq 0\}$$

is globalized to obtain the *unstable manifold*

$$W^u(p) := \bigcup_{n \geq 0} f^n(W_{\text{loc}}^u(p)). \quad (7)$$

Both  $W^s(p)$  and  $W^u(p)$  are immersed manifolds with dimensions given by the number of eigenvalues of modulus less than and larger than 1, respectively [26]. A one-dimensional global manifold is a curve that consists of two branches on either side of  $p$ ; each branch can be parametrized by arclength.

A starting point of our study are the global manifolds  $W^s(p_h^\pm)$  and  $W^u(p_h^\pm)$  of the saddle points  $p_h^\pm$  of the two-dimensional Hénon map  $h$  for  $\mu = -9.5$  and  $\beta = 0.1$ . They are both one-dimensional curves and are shown in figure 1 on the Poincaré disk  $\mathcal{D}$ . Shown are the boundary  $\partial\mathcal{D}$  (black circle) containing the sink  $q_h$  (blue triangle) and the source  $s_h$  (red square), the saddle fixed points  $p_h^+$  and  $p_h^-$  (green crosses), their stable manifolds  $W^s(p_h^+)$  (blue) and  $W^s(p_h^-)$  (cyan), and their unstable manifolds  $W^u(p_h^-)$  (red) and  $W^u(p_h^+)$  (magenta). The inset shows an enlargement of the global manifolds near the fixed point  $p_h^-$ . The manifolds  $W_h^s(p^\pm)$  and  $W_h^u(p^\pm)$  intersect transversally in the hyperbolic set that contains  $p_h^+$  and  $p_h^-$ , forming a homoclinic tangle. Therefore, the structure of  $W_h^s(p^\pm)$  and  $W_h^u(p^\pm)$  is locally that of a Cantor set times curve segments. Note that the (un)stable manifolds of  $p_h^+$  and  $p_h^-$  lie so close together that they are difficult to distinguish in figure 1.

The homoclinic tangle involves excursions of the manifolds closer and closer to infinity, that is to the boundary  $\partial\mathcal{D}$  of the Poincaré disk; more specifically,  $W_h^s(p^\pm)$  accumulates on the source  $s_h$  and  $W_h^u(p^\pm)$  accumulates on the sink  $q_h$ . Considering the dynamics on the compactified phase space, such as the Poincaré disk  $\mathcal{D}$  shown in figure 1, not only allows one to observe the overall dynamics globally, but it also has the major advantage that excursions of the global manifolds to near infinity do not result in a massive increase in their arclengths; indeed, every excursion to near  $s_h$  and  $q_h$ , respectively, is associated with a bounded arclength.

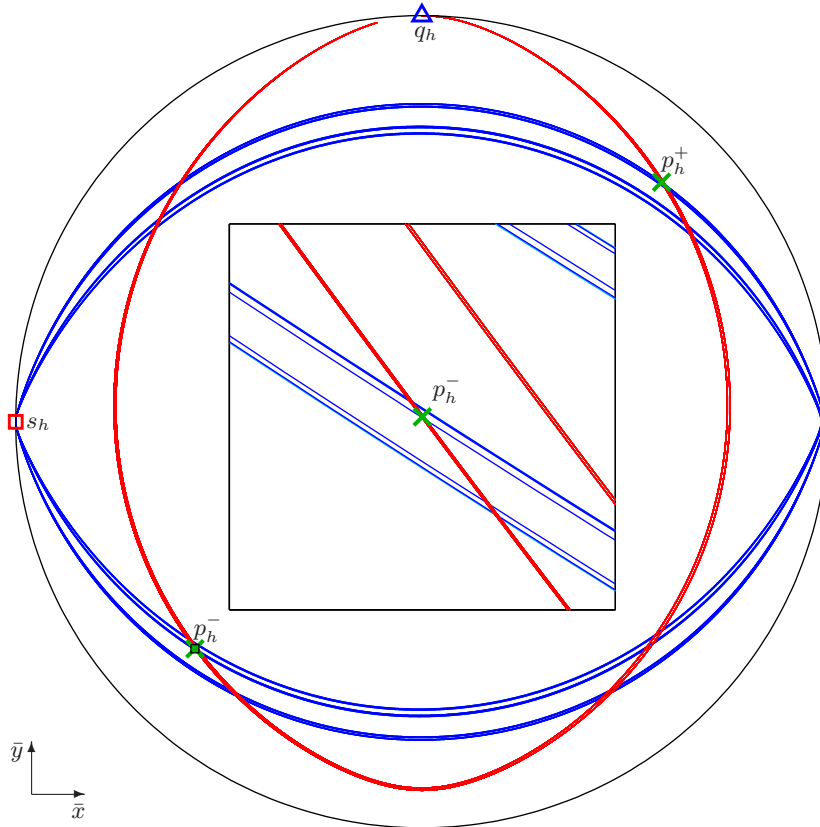


Figure 1: Homoclinic tangle of the two-dimensional Hénon map (2) for  $\mu = -9.5$  and  $\beta = 0.1$  on the Poincaré disk  $\mathcal{D}$ . Shown are  $\partial\mathcal{D}$  (black unit circle), the sink  $q_h \in \partial\mathcal{D}$  (blue triangle), the source  $s_h \in \partial\mathcal{D}$ , the saddle fixed points  $p_h^+$  and  $p_h^-$  (green crosses), and their stable and unstable manifolds  $W^s(p_h^\pm)$  (blue and cyan) and  $W^u(p_h^\pm)$  (red and magenta), computed up to arclength  $L = 100$ .

This is a considerable advantage for the computation and representation of global invariant manifolds. Indeed, except in very special and untypical circumstances, analytical expressions do not exist for global stable and unstable manifolds. Hence, they need to be approximated numerically, even when they are of dimension one. The basic idea is to compute a one-dimensional global manifold, say,  $W^s(p)$  of a saddle equilibrium  $p$ , as a curve up to a prespecified finite arclength. Technically speaking, for given  $L \geq 0$  we consider the first piece  $W_L^s(p)$  of all points of  $W^s(p)$  that have an arclength (or geodesic) distance at most  $L$  to  $p$  along the manifold [19]. Note that a one-dimensional manifold  $W_L^s(p)$  consists of two curves or branches of arclength  $L$  on either side of  $p$ . The first piece  $W_L^u(p) \subset W^u(p)$  of a one-dimensional unstable manifold is defined in the same way.

The important point is that the finite one-dimensional objects  $W_L^s(p)$  and  $W_L^u(p)$  can be computed efficiently and accurately, that is, with established error bounds [19]. We compute the respective approximations with the method introduced in [19] and implemented in the DS TOOL environment [1]. The underlying idea is that each branch of the manifold is grown from  $p$  up to the total given arclength  $L$  by adding, at each step, a new point that lies on the manifold to good approximation; the mesh, that is, the distance between consecutive points of this sequence, is adapted with the curvature of the manifold according to user-specified accuracy parameters. The thus obtained sequence of points defines a piecewise-linear curve that represents the respective branch of the one-dimensional manifold. More details can be

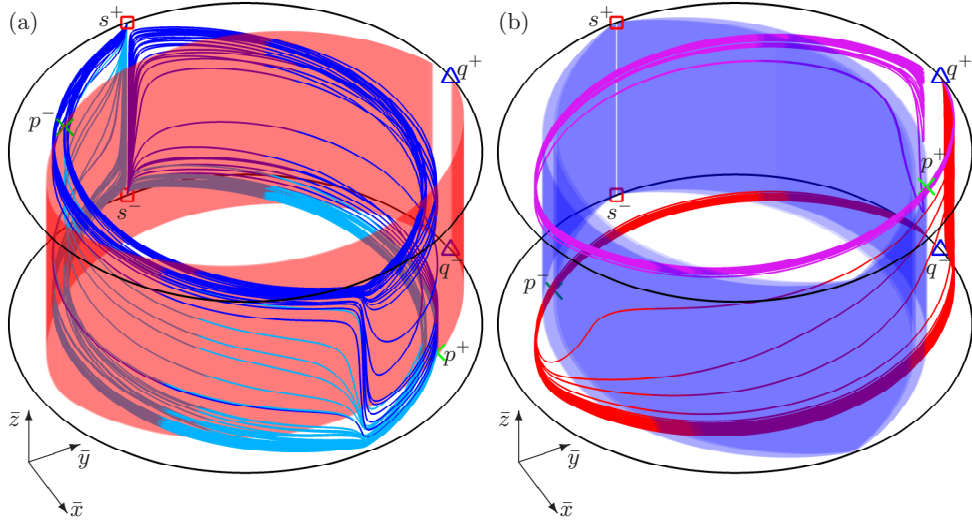


Figure 2: The global manifolds  $W^s(p^\pm)$  and  $W^u(p^\pm)$  of (1) with  $\mu = -9.5$  and  $\beta = 0.1$  in the cylinder  $\mathcal{C}$  for  $\xi = 1.185$  (a) and for  $\xi = 0.9$  (b). Shown are the two bounding circles (black) of  $\mathcal{C}$ , the sinks  $q^\pm$  (blue triangles) and the sources  $s^\pm$  (red squares) on them, the saddle fixed points  $p^\pm$  (green crosses), and their stable and unstable manifolds  $W^s(p^\pm)$  (cyan and blue) and  $W^u(p^\pm)$  (magenta and red), computed up to arclength  $L = 200$  when of dimension one and up to  $L = 50$  when of dimension two.

found in Appendix A. The global manifolds shown in figure 1 are the approximations of  $W_L^s(p_h^\pm)$  and  $W_L^u(p_h^\pm)$  with  $L = 100$ , where the arclength  $L$  is in terms of the Euclidean distance on  $\mathcal{D} \subset \mathbb{R}^2$ . For notational simplicity we generally refer to these approximations as  $W^s(p_h^\pm)$  and  $W^u(p_h^\pm)$  computed up to the stated arclength  $L$  (and similarly to other computed one-dimensional manifolds) unless the context requires the subscript  $L$ .

We now consider the global invariant manifolds of the equilibria  $p^\pm$  of the three-dimensional map (1) for  $\mu = -9.5$  and  $\beta = 0.1$  in the compactified phase space  $\mathcal{C}$ . Since  $\xi$  is one of the eigenvalues of  $p^\pm$  the manifolds  $W^s(p^\pm)$  and  $W^u(p^\pm)$  are one dimensional or two dimensional depending on whether  $\xi$  is larger or smaller than 1. Moreover, irrespective of their dimensions, their projections onto  $\mathcal{D}$  are the global manifolds  $W^s(p_h^\pm)$  and  $W^u(p_h^\pm)$  from figure 1. Namely, we have the following.

$$\begin{aligned} \text{For } \xi > 1: \quad & \dim(W^s(p^\pm)) = 1 \text{ and } W^u(p^\pm) = W_h^u(p_h^\pm) \times (-1, 1); \\ \text{For } \xi < 1: \quad & W^s(p^\pm) = W_h^s(p_h^\pm) \times (-1, 1) \text{ and } \dim(W^u(p^\pm)) = 1. \end{aligned}$$

Hence, we compute the one-dimensional manifolds  $W^s(p^\pm)$  for  $\xi > 1$  and  $W^u(p^\pm)$  for  $\xi < 1$  as curves up to a given arclength  $L$ , where the arclength is now in terms of the Euclidean distance on  $\mathcal{C} \subset \mathbb{R}^3$ . The two-dimensional manifolds  $W^u(p^\pm)$  for  $\xi > 1$  and  $W^s(p^\pm)$  for  $\xi < 1$  are rendered as surfaces in  $\mathcal{C}$  from the respective computed one-dimensional manifolds  $W_h^u(p_h^\pm)$  and  $W_h^s(p_h^\pm)$  of the Hénon map  $h$  up to arclength  $L$ . Figure 2 shows these invariant manifolds of  $H$  in the cylinder  $\mathcal{C}$  for  $\xi = 1.185$  in panel (a) and for  $\xi = 0.9$  in panel (b), where  $L$  has the moderate value  $L = 50$ . The cylinder is delimited by the two boundary circles shown, which contain the equilibria at infinity, namely, the sinks  $q^\pm$  and the sources  $s^\pm$ . Note that for  $\xi = 1.185 > 1$  in panel (a) the  $z$ -coordinates of  $p^+$  and  $p^-$  are positive and negative, whereas for  $\xi = 0.9 < 1$  in panel (b) they are negative and positive, respectively. More specifically, figure 2(a) shows, for  $\xi = 1.185$ , the one-dimensional stable manifolds  $W^s(p^-)$  (blue) and  $W^s(p^+)$  (cyan) and the two-dimensional unstable manifold  $W^u(p^-)$  (red). Notice that the curves  $W^s(p^\pm)$  cover a wide range of  $\bar{z}$ -values and make excursions very close to both sources

$s^\pm$ . Similarly, panel (b) shows, for  $\xi = 0.9$ , the two-dimensional stable manifold  $W^s(p^-)$  (blue) and the one-dimensional unstable manifolds  $W^u(p^-)$  (magenta) and  $W^u(p^+)$  (red), which also cover a wide range of  $\bar{z}$ -values and make excursions very close to both sinks  $q^\pm$ .

## 2.5 The carpet property

We consider the simplest case of a three-dimensional diffeomorphism from now on. In this setting blenders have been defined in two ways. We speak of a *phenomenological blender* when a hyperbolic set generated by a horseshoe satisfies the sufficient condition in [5], and of a *conceptual blender* when the more general definition from section 2.1 is satisfied. We consider the latter case throughout this paper and, hence, say that a hyperbolic set  $\Lambda \subset \mathbb{R}^3$  of unstable index  $k = 2$  is a blender if there is a  $C^1$ -open set of one-dimensional manifolds (curve segments) that each intersect the one-dimensional local stable manifold  $W_{\text{loc}}^s(\Lambda)$ ; this property must hold for every sufficiently  $C^1$ -close diffeomorphism. Similarly, we also refer to  $\Lambda \subset \mathbb{R}^3$  as a blender if it has unstable index  $k = 1$ , there is a  $C^1$ -open set of curve segments that each intersect the local unstable manifold  $W_{\text{loc}}^u(\Lambda)$  and this property is robust; hence, this is simply a blender for the inverse map.

Therefore, the one-dimensional local stable or unstable manifolds of a blender in a three-dimensional diffeomorphism ‘looks’ like a two-dimensional surface when viewed from an open set of appropriate directions, given by tangents to the  $C^1$ -open set of curve segments in the definition. We refer to this defining property of the one-dimensional (un)stable manifold of such a blender as the *carpet property*; after all, in a carpet one-dimensional strings are interwoven so closely that they form a surface when viewed from an open set of directions.

The carpet property effectively says that the closure of the two-dimensional projection of  $W^s(\Lambda)$  or  $W^u(\Lambda)$  along a fixed, suitable direction has non-empty interior. Moreover, this property persists in an open neighbourhood of directions of projection. The idea of this paper is to devise a numerical scheme to check this projection property in an effective and accurate way.

To determine the suitable direction of projection, we make use of the properties of the map under consideration. For  $\mu \in (-10, -9)$ , small  $\beta$ , and  $\xi > 1$  the blender in the map (1) is formed by the lift of the stable manifold of the hyperbolic set of the two-dimensional Hénon map (2); see figure 1. In particular, the strong unstable subspace of (1) is mostly parallel to the  $y$ -axis, so that (an open set around) the  $y$ -direction emerges as the relevant direction of projection. Note that this property is preserved under compactification of the phase space, which is why we will consider projection along the  $\bar{y}$ -axis of the cylinder  $\mathcal{C}$ . For  $\xi < 1$  the blender is formed by the lift of the unstable manifold of the hyperbolic set of (2), and the natural projection direction is given similarly by the  $\bar{x}$ -axis; see again figure 1.

It is not possible to compute the one-dimensional invariant manifold  $W^s(\Lambda)$  in its entirety, that is, all of the stable manifolds of its uncountably many constituent points. To overcome this issue, we make use of the fact that periodic points are dense in the hyperbolic set  $\Lambda$ ; this is indeed the case for map (1) because, as was mentioned in section 2.2,  $\Lambda$  is generated by a full horseshoe and the dynamics on it is conjugate to a full shift on two symbols. We consider a periodic point of lowest period, which for (1) we choose to be the fixed point  $p^- \in \Lambda$ . Since all hyperbolic periodic points in  $\Lambda$  are connected by heteroclinic orbits, any periodic point lies in the closure of the one-dimensional manifold  $W^s(p^-)$ . This implies that, for (1) with  $\xi > 1$ , the single one-dimensional immersed manifold  $W^s(p^-)$  is dense in  $W^s(\Lambda)$ . Hence, we can check for the carpet property by determining whether the projection of  $W^s(p^-)$  along the  $\bar{y}$ -axis onto the  $(\bar{x}, \bar{z})$ -plane fills an open region densely, and that this property persists under small variations of the projection angle. This is what we demonstrate in the next section. In section 4, we will then check similarly the carpet property for  $\xi < 1$  by testing for the denseness of  $W^u(p^-)$  in

projection along  $\bar{x}$  onto the  $(\bar{y}, \bar{z})$ -plane under different projection angles.

### 3 The blender and its transition for $\xi > 1$

To check numerically that the map  $H$  does have a blender for  $\mu = -9.5$ ,  $\beta = 0.1$  and  $\xi = 1.185$ , we now compute the one-dimensional stable manifold  $W^s(p^-)$  up to much larger arclength  $L$ . We show  $W^s(p^-)$  in different projections and then provide numerical evidence for the carpet property by computing the maximal gap between the points in a certain subsection in different projections, and as a function of  $L$ ; see section 3.2. In section 3.3 we then check for the carpet property as  $\xi > 1$  is increased.

#### 3.1 The blender for $\xi = 1.185$

Figure 3 is the first picture of a blender and its stable manifold in an explicitly defined diffeomorphism. Specifically, for  $H$  with  $\mu = -9.5$ ,  $\beta = 0.1$  and  $\xi = 1.185$ , it shows the one-dimensional stable manifold  $W^s(p^-)$  in  $\mathcal{C}$ , now computed up to arclength  $L = 4800$ ; note that this is a considerable arclength, given that  $\mathcal{C}$  has a diameter and height of 2. Moreover, to illustrate its structure,  $W^s(p^-)$  is coloured as follows: for each curve segment of  $W^s(p^-)$  starting near the points  $s^\pm$  and ending in the half-plane given by  $\bar{y} = 0$  for  $\bar{x} > 0$ , we determine the maximal value of  $|\bar{y}|$ ; this maximal value is then used to colour the segment, from dark green for the smallest maximal  $|\bar{y}|$ -value to blue for the largest. Figure 3 (a) shows the bounding circles in  $\partial\mathcal{C}$ , the sources  $s^\pm$ , the saddle fixed point  $p^-$  and  $W^s(p^-)$ . Panel (b) shows the projection onto the disk  $\mathcal{D}$ , which illustrates the Cantor-set structure of  $W^s(p^-)$  and how it is reflected in the colour scheme; compare with figure 1. Figure 3(c) shows the projection of  $\mathcal{C}$  in the  $\bar{y}$ -direction onto the  $(\bar{x}, \bar{z})$ -plane  $[-1, 1] \times [-1, 1]$ , which illustrates the carpet property of  $W^s(p^-)$ . More precisely, it appears that  $W^s(p^-)$  is filling an entire region densely. Notice that the curve segments of  $W^s(p^-)$  align along the  $\bar{x}$ -direction near  $\bar{x} = 0$  in the centre of panel (c). Since the computation is for the finite arclength  $L = 4800$ , there are still gaps in between the different curve segments, but they appear to be distributed over a large range of  $\bar{z}$ -values with slightly larger gaps near  $\bar{z} = 0$ . Moreover, during the computation, new segments of  $W^s(p^-)$  divide up the remaining gaps to bring the overall gap size down. Hence, figure 3 constitutes a strong indication that the closure  $\overline{W^s(p^-)}$  is the stable manifold of a blender of  $H$  for  $\xi = 1.185$ .

#### 3.2 Computing the maximal gap

We now present a numerical method to measure the *maximal gap* between segments of  $W^s(p^-)$  when computed up to arclength  $L$ . Its convergence as a function of the arclength  $L$  will allow us to determine denseness and, hence, whether or not  $W^s(p^-)$  has the carpet property; see section 2.5.

Guided by figure 3 we consider  $W^s(p^-)$  up to a given  $L$  and measure the gaps between segments of  $W^s(p^-)$  in the  $\bar{y}$ -direction for  $\bar{x} = 0$ . To this end, we consider its intersection set with the plane  $\Sigma := \{(\bar{x}, \bar{y}, \bar{z}) : \bar{x} = 0\}$ , which is illustrated in figure 4 for  $\xi = 1.185$  and  $L = 4800$ . In order to check for denseness, we now consider the  $N_L$  intersection points of the approximation of  $W^s(p^-)$  with the half-plane  $\Sigma^+ := \{(\bar{x}, \bar{y}, \bar{z}) : \bar{x} = 0, \bar{y} > 0\}$ , which we take to be ordered for increasing values of  $\bar{z}$ , that is,

$$W_L^s(p^-) \cap \Sigma^+ = \{(0, \bar{y}_i, \bar{z}_i) \in W_L^s(p^-) \mid \bar{z}_i \leq \bar{z}_{i+1} \text{ for } 1 \leq i \leq N_L - 1\}.$$

Then the *maximal gap* for the projection in the  $\bar{y}$ -direction is given as

$$\Delta_L := \max\{\bar{z}_{i+1} - \bar{z}_i \mid 1 \leq i \leq N_L - 1\}. \quad (8)$$

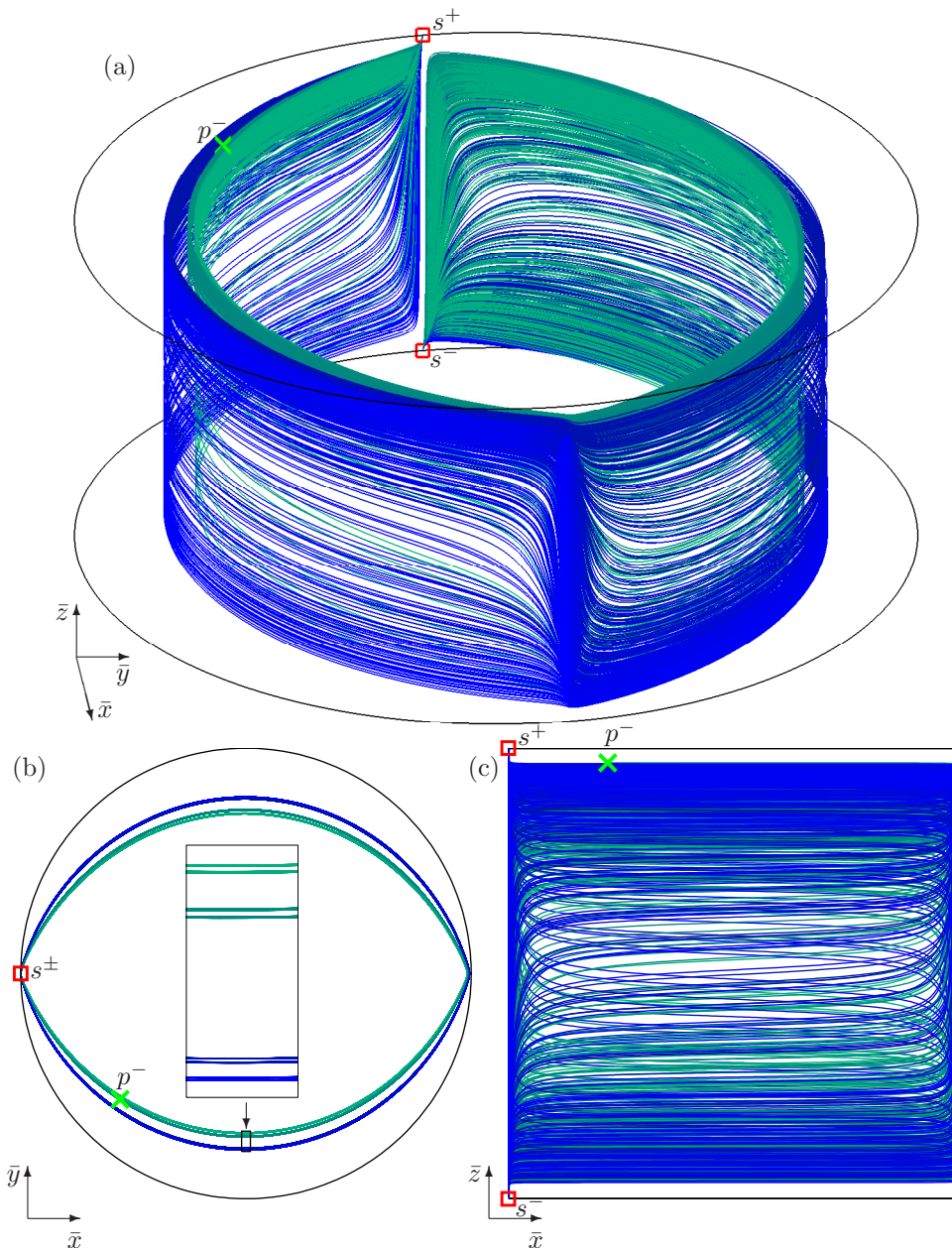


Figure 3: The stable manifold  $W^s(p^-)$  of  $H$  for  $\xi = 1.185$ , computed up to arclength  $L = 4800$ , shown in  $\mathcal{C}$  (a) and in projections onto  $\mathcal{D}$  (b) and the  $(\bar{x}, \bar{z})$ -plane (c); here  $\mu = -9.5$ ,  $\beta = 0.1$ .

Note that both  $N_L$  and  $\Delta_L$  depend on the arclength  $L$  (as well as on all system parameters). Our numerical computations show that, for the values of  $\mu$ ,  $\beta$  and  $\xi$  considered here, the number  $N_L$  of intersections grows linearly with  $L$ . To determine the convergence of  $\Delta_L$  to zero as  $L$  increases we consider  $L = 600 \cdot 2^k$ , for which we find  $N_L \approx 88 \cdot 2^k$ . We then plot the maximal gap as a function of the exponent  $k$  up to  $k = 12$ ; note that the latter corresponds to an arclength of  $L = 2,457,600$  inside the  $2 \times 2$  cylinder  $\mathcal{C}$ !

Figure 5 shows the maximal gap  $\Delta_L$  as a function of  $k$  for  $\xi = 1.185$  on a linear scale in panel (a) and on a logarithmic scale in panel (b), which allows us to observe that  $\Delta_L$  goes to zero for increasing  $k$  and that this decay is approximately exponential. This agrees with our initial observation from figure 3 that  $W^s(p^-)$  fills up an open region in the  $\bar{y}$ -projection. Hence, figure 5 provides strong numerical evidence for the carpet property.

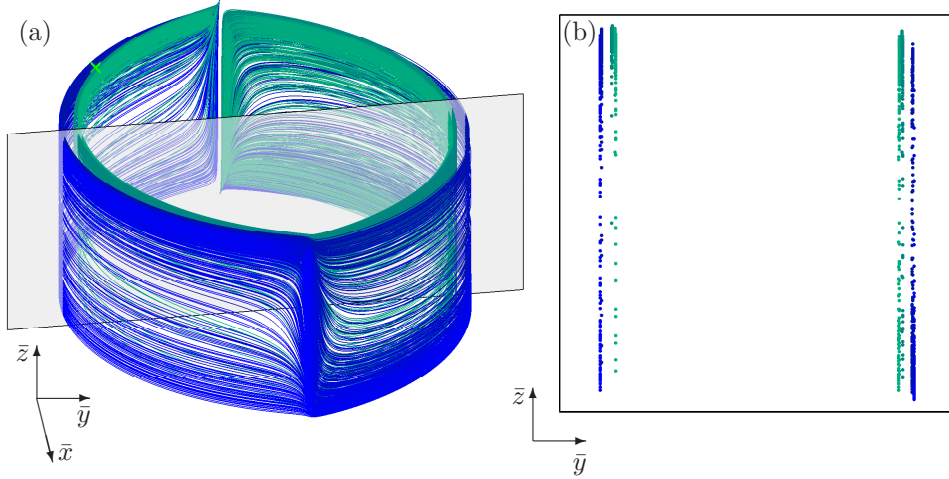


Figure 4: The stable manifold  $W^s(p^-)$  of  $H$  for  $\xi = 1.185$  with the plane  $\Sigma$  given by  $\bar{x} = 0$  (a) and their intersection set in  $\Sigma$  (b); here  $\mu = -9.5$ ,  $\beta = 0.1$  and  $L = 4800$ .

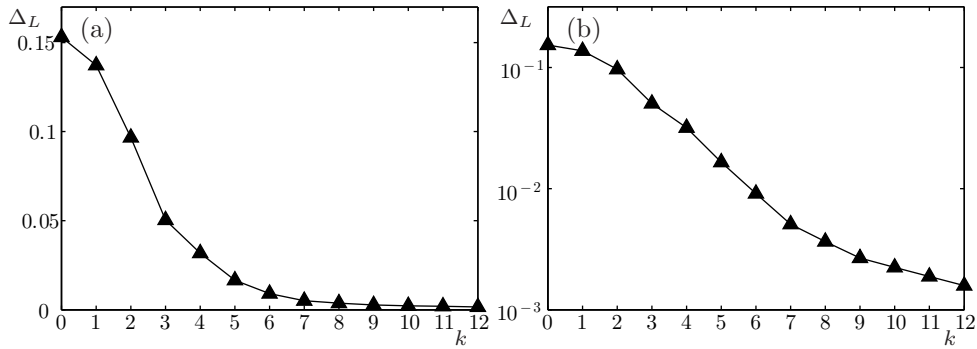


Figure 5: Maximal gap  $\Delta_L$  of  $W_L^s(p^-) \cap \Sigma^+$  for  $\xi = 1.185$  as a function of  $k$  with  $L = 600 \cdot 2^k$ , shown on a linear  $\Delta_L$ -scale (a) and a logarithmic  $\Delta_L$ -scale (b); here  $\mu = -9.5$  and  $\beta = 0.1$ .

To check that this property persists under variations of the direction of projection, we consider the projection

$$\rho_\alpha(\bar{y}, \bar{z}) = \sin\left(\frac{\pi}{2}\alpha\right)\bar{y} + \cos\left(\frac{\pi}{2}\alpha\right)\bar{z}$$

of points  $(0, \bar{y}, \bar{z}) \in W_L^s(p^-) \cap \Sigma^+$  in the direction given by the angle  $\alpha$  in the plane  $\Sigma$ . We now order the points in  $W_L^s(p^-) \cap \Sigma^+$  by their projection  $\rho_\alpha$ , that is, we write

$$W_L^s(p^-) \cap \Sigma^+ = \{(0, \bar{y}_i, \bar{z}_i) \in W_L^s(p^-) \mid \rho_\alpha(\bar{y}_i, \bar{z}_i) \leq \rho_\alpha(\bar{y}_{i+1}, \bar{z}_{i+1}) \text{ for } 1 \leq i \leq N_L - 1\},$$

where  $N_L$  is the number of points in  $W_L^s(p^-) \cap \Sigma^+$  as above. The *maximal gap for the projection angle*  $\alpha$  is then defined as

$$\Delta_L^\alpha := \max\{\rho_\alpha(\bar{y}_{i+1}, \bar{z}_{i+1}) - \rho_\alpha(\bar{y}_i, \bar{z}_i) \mid 1 \leq i \leq N_L - 1\}.$$

Note that, in particular,  $\Delta_L^0 = \Delta_L$ ; moreover, it suffices to consider only  $\alpha \in [0, 1]$ , that is, in between the horizontal and the vertical projection.

Figure 6 shows the maximal gap  $\Delta_L^\alpha$  as a function of the projection angle  $\alpha \in [0, 1]$  for  $\xi = 1.185$ . Here  $W_L^s(p^-)$  is computed up to arclength  $L = 600 \cdot 2^{10}$ ; this choice is based on figure 5, which shows that  $\Delta_L$  changes only very little for  $k \geq 10$ . In figure 6 we computed  $\Delta_L^\alpha$  for 101 linearly distributed angles  $\alpha \in [0, 0.5]$ . We find that  $\Delta_L^0 \approx 0.00224$  and that  $\Delta_L^\alpha$  is

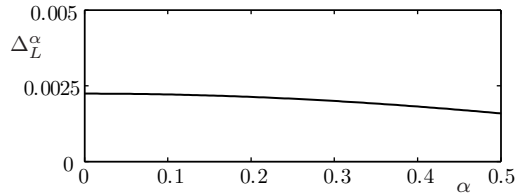


Figure 6: Maximal gap  $\Delta_L^\alpha$  of  $W_L^s(p^-) \cap \Sigma^+$  for  $\xi = 1.185$  as a function of the projection angle  $\alpha \in [0, 0.5]$ ; here  $\mu = -9.5$ ,  $\beta = 0.1$  and  $L = 600 \cdot 2^{10}$ .

monotonically decreasing for  $\alpha \in [0, 0.5]$ . This is evidence that, for fixed  $\alpha$  near zero,  $\Delta_L^\alpha$  also converges to zero with increasing  $L$ .

Taken together, the computations of  $\Delta_L$  for increasing  $k$  in figure 5 and of  $\Delta_L^\alpha$  for increasing  $\alpha$  in figure 6 constitute convincing numerical evidence for the carpet property. In turn, this demonstrates that the map  $H$  for  $\xi = 1.185$  does have a blender, as was conjectured based on the related results in [11]. Following our numerical results, the blender property of  $H$  for  $\xi = 1.185$ ; was subsequently proved; the proof is technical and adapted from the proof for (3) from [11], which is why we placed it in Appendix A.

### 3.3 The transition of the blender for $\xi > 1$

An advantage of our numerical approach is that it allows us to study the persistence and/or disappearance of the blender for increasing  $\xi > 1$ . Figures 7–9 show what happens to the blender for  $\xi = 1.185$  from figure 3 when  $\xi$  is increased to  $\xi = 1.6$ , 2 and 2.6, respectively. These figures show  $W^s(p^-)$  computed up to arclength  $L = 4800$  in  $\mathcal{C}$ , in projection onto  $\mathcal{D}$  and in projection onto the  $(\bar{x}, \bar{z})$ -plane in panels (a)–(c), respectively. Note that the projections onto  $\mathcal{D}$  do not change. However, we observe definite changes in the structure of  $W^s(p^-)$  in panels (a) and (c).

In figure 7(a), where  $\xi = 1.6$ , we notice that the inner (dark green) segments and the outer (blue) segments of  $W^s(p^-)$  (blue) have separated; compare with figure 3(a). By this we mean that the inner segments admit a large range of  $\bar{z}$ -values for  $\bar{y} > 0$  and a small range of  $\bar{z}$ -values for  $\bar{y} < 0$ , whereas it is the other way around for the outer segments of  $W^s(p^-)$ . Nevertheless, in figure 7(c) we hardly observe any gaps between the segments of  $W^s(p^-)$  when computed up to  $L = 4800$ , and after they have been projected onto the  $(\bar{x}, \bar{z})$ -plane. In other words, we expect that the carpet property is still satisfied, meaning that  $H$  still has a blender for  $\xi = 1.6$ .

When  $\xi$  is increased to  $\xi = 2.0$ , on the other hand, as in figure 8, the inner and outer segments of  $W^s(p^-)$  have separated further and now span a much smaller range of  $\bar{z}$ -values. Moreover, obvious gaps have appeared in the projection onto the  $(\bar{x}, \bar{z})$ -plane in panel (c). It appears that these gaps are distributed over the range of  $\bar{z}$ -values in what looks like a Cantor-set structure. We checked that the visible gaps in the  $(\bar{x}, \bar{z})$ -plane do not decrease when  $W^s(p^-)$  is computed for increasing  $L$  (not shown). Overall, figure 8 suggests that the carpet property is no longer satisfied, meaning that  $H$  no longer has a blender. This suggestion is supported by figure 9 for  $\xi = 2.5$ , where the observed Cantor-set structure of  $W^s(p^-)$  is much thinner in panel (a), and there is a clear hierarchy of gaps in the projection in panel (c).

Overall, although we computed  $W^s(p^-)$  only up to arclength  $L = 4800$ , figures 7–9 are numerical evidence that the carpet property is initially still satisfied, and a blender exists when  $\xi$  is increased from  $\xi = 1.185$ , while this property is lost when  $\xi$  becomes too large. The transition constitutes a novel type of global bifurcation of the system in the form of the destruction/creation of a blender. The exact nature of this bifurcation merits further research. At this stage, it is not entirely clear what the new properties of  $W^s(p^-)$  are past this bifurcation. More precisely, also when projected onto the  $(\bar{x}, \bar{z})$ -plane,  $W^s(p^-)$  seems to admit

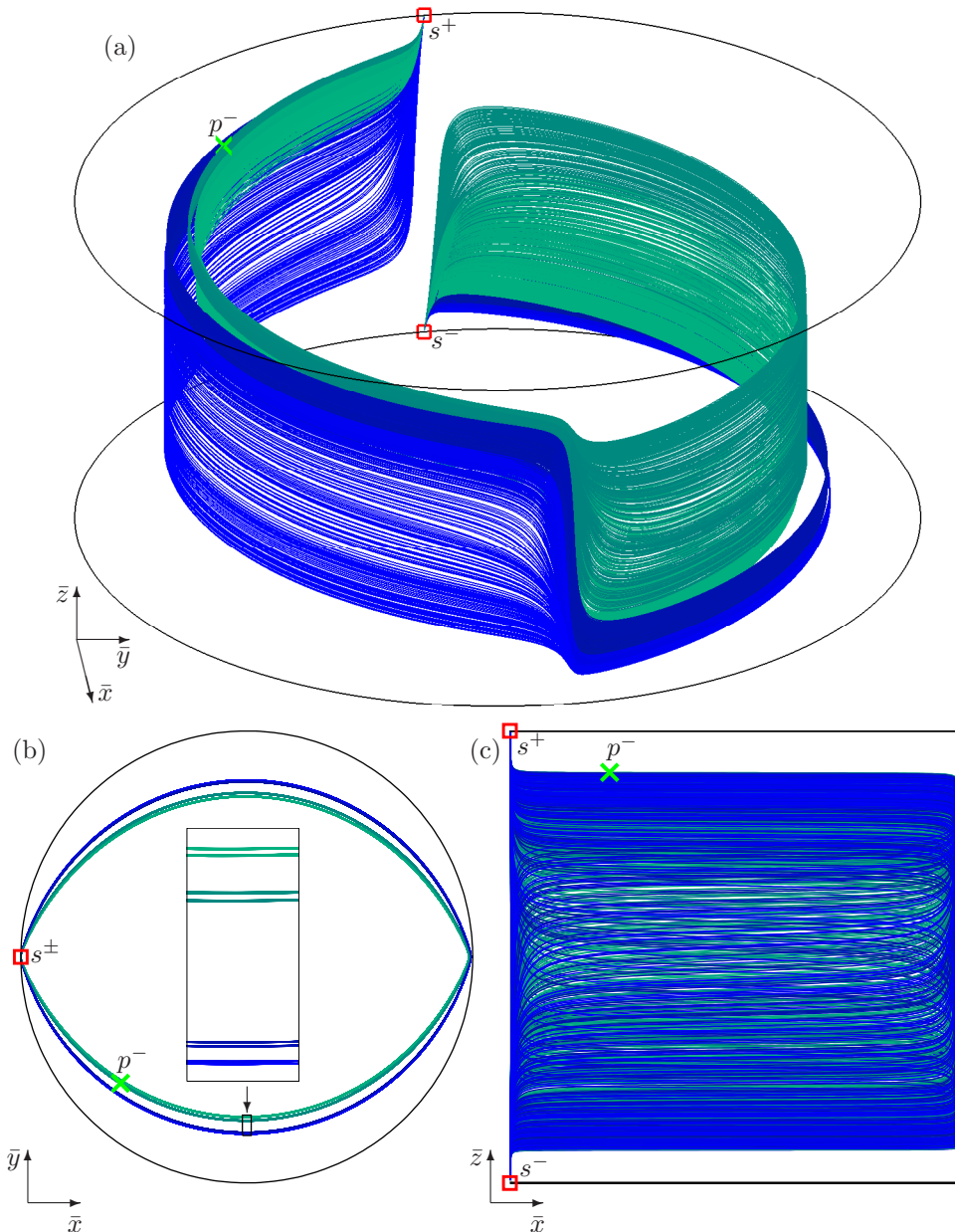


Figure 7: The stable manifold  $W^s(p^-)$  of  $H$  for  $\xi = 1.6$ , computed up to arclength  $L = 4800$ , shown in  $\mathcal{C}$  (a) and in projections onto  $\mathcal{D}$  (b) and the  $(\bar{x}, \bar{z})$ -plane (c); here  $\mu = -9.5$ ,  $\beta = 0.1$ .

a Cantor-set structure, but we cannot yet exclude the possibility that there are small strips that might have the carpet property locally at a much smaller scale; see, already, section 5.1.

We present in figure 10 more substantial numerical evidence for the existence or non-existence of the blender for  $\xi > 1$ . More specifically, the maximal gap  $\Delta_L$  is shown as a function of  $k$  with  $L = 600 \cdot 2^k$  for  $\xi = 1.185$  (triangles),  $\xi = 1.6$  (squares),  $\xi = 2.0$  (circles) and  $\xi = 2.5$  (diamonds). Panel (a) shows  $\Delta_L$  on a linear scale and panel (b) shows it on a logarithmic scale; compare with figure 5. Figure 10 clearly shows that  $\Delta_L$  decays exponentially for  $\xi = 1.185$  and  $\xi = 1.6$ , whereas  $\Delta_L$  converges rapidly to fixed positive values  $\Delta_L \approx 0.0835$  for  $\xi = 2.0$  and  $\Delta_L \approx 0.1642$  for  $\xi = 2.5$ . These findings clearly confirm our initial observations that  $W^s(p^-)$  has the carpet property for  $\xi = 1.185$  and  $\xi = 1.6$ , but not for  $\xi = 2$  and  $\xi = 2.5$ .

Again, for each of these  $\xi$ -values the maximal gap  $\Delta_L$  changes very little for  $k \geq 10$  in

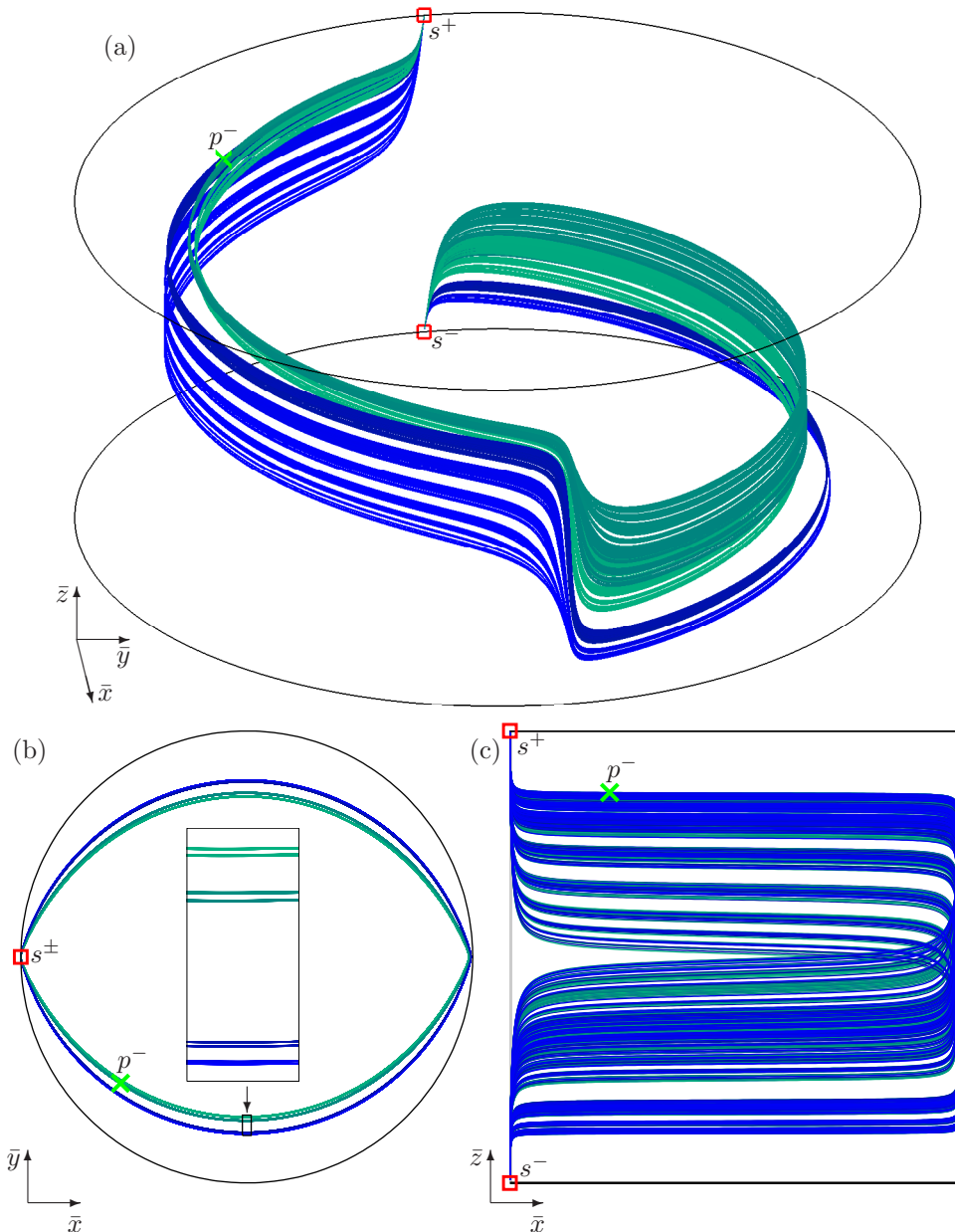


Figure 8: The stable manifold  $W^s(p^-)$  of  $H$  for  $\xi = 2.0$ , computed up to arclength  $L = 4800$ , shown in  $\mathcal{C}$  (a) and in projections onto  $\mathcal{D}$  (b) and the  $(\bar{x}, \bar{z})$ -plane (c); here  $\mu = -9.5$ ,  $\beta = 0.1$ .

figure 10(a), so we again choose the arclength  $L = 600 \cdot 2^{10}$  to determine its dependence on  $\xi$ . Figure 11 shows  $\Delta_L$  (black) for fixed  $L = 600 \cdot 2^{10}$  over the range  $\xi \in [1.05, 2.5]$  on a linear scale in panel (a) and on a quadratic scale in panel (b); the black dots in the figure correspond to the computed values of  $\Delta_L$  for the respective values of  $\xi$ . We observe that  $\Delta_L$  is very small and, in fact, decreasing to about  $10^{-4}$  for  $\xi \in [1.1, 1.74]$ . It then increases considerably for  $\xi > 1.74$ , initially slowly but subsequently in a seemingly square-root fashion. Correspondingly, the plot on the quadratic scale is about linear for  $\xi \geq 1.8$  and we show in panel (b) the least-squares regression line (grey) for the data points at  $\xi \in \{1.9, 1.95, 2, 2.1, 2.2, 2.3\}$ , which corresponds to a square-root curve (grey) on the linear scale in panel (a). One expects this curve only to be a good approximation sufficiently close to the bifurcation, where the carpet property is lost; moreover, it is to be expected that the convergence of  $\Delta_L$  to zero slows down the closer  $\xi$  is to

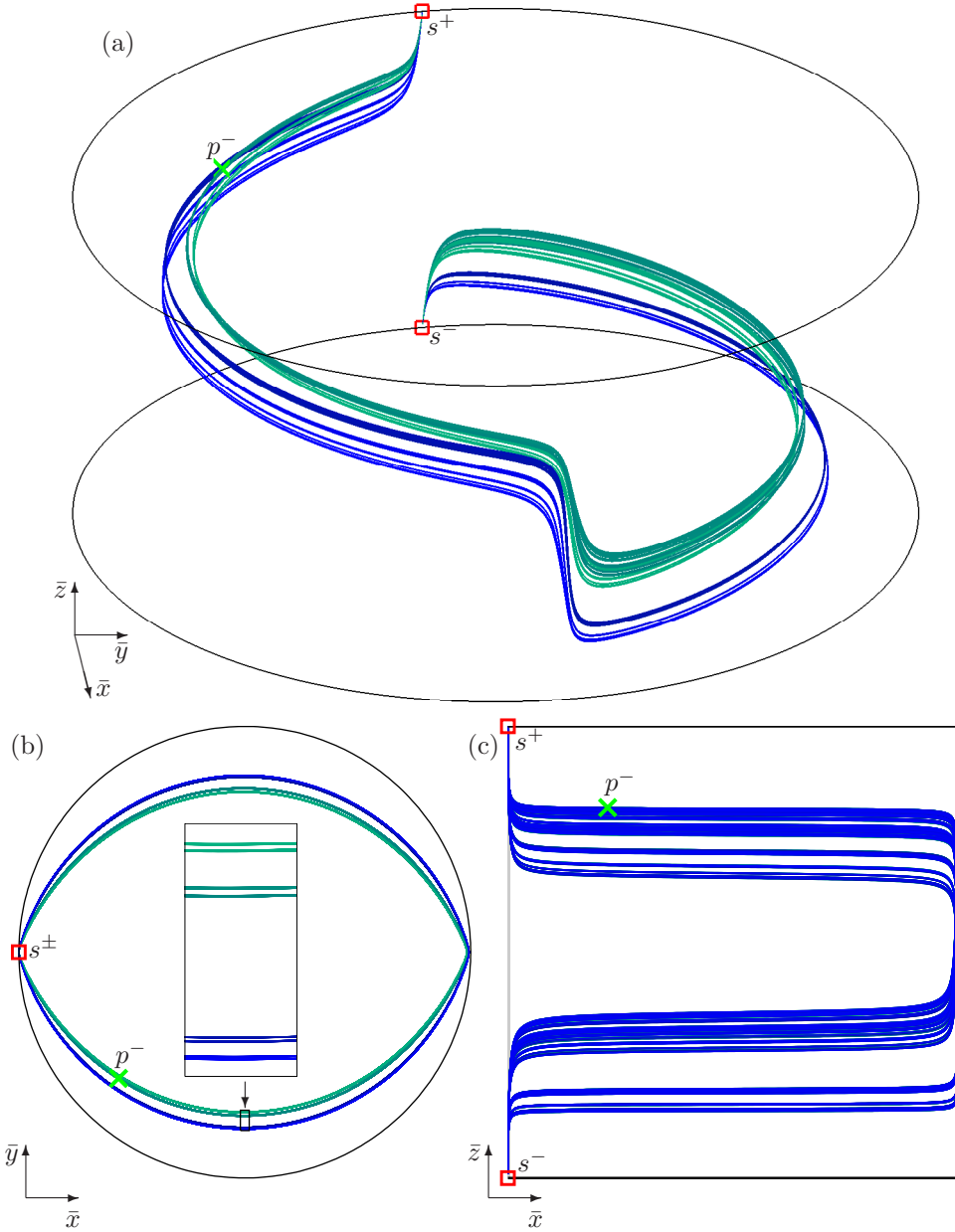


Figure 9: The stable manifold  $W^s(p^-)$  of  $H$  for  $\xi = 2.5$ , computed up to arclength  $L = 4800$ , shown in  $\mathcal{C}$  (a) and in projections onto  $\mathcal{D}$  (b) and the  $(\bar{x}, \bar{z})$ -plane (c); here  $\mu = -9.5$ ,  $\beta = 0.1$ .

the bifurcation value. We therefore suspect that the carpet property is lost and the blender is destroyed near the value  $\xi^* := 1.843$ , where the regression line in figure 11(b) crosses zero.

One of the important ingredients for the proof of existence of blenders in [5, 8, 7] is the existence of a *centre-unstable direction*, that is, the expansion rate in this direction is relatively weaker than in the other directions. Thus, from the theoretical viewpoint we expect the existence of blenders in the map  $H$  when  $\xi \approx 1$ . On the other hand, the computed quantity  $\Delta_L$  for fixed  $L = 600 \cdot 2^{10}$  increases somewhat when  $\xi = 1$  is approached in figure 11. This happens because  $\xi$  is the eigenvalue of the fixed point  $p^-$  in the  $z$ -direction. As a result, when  $\xi$  is close to 1, the stable manifold  $W^s(p^-)$  covers the required and large  $\bar{z}$ -range much more slowly. This can be seen when comparing figure 3(c) with figure 7(c), where the largest gap for fixed  $L = 4800$  is noticeably larger for  $\xi = 1.185$  than for  $\xi = 1.6$ . In other words, the gaps

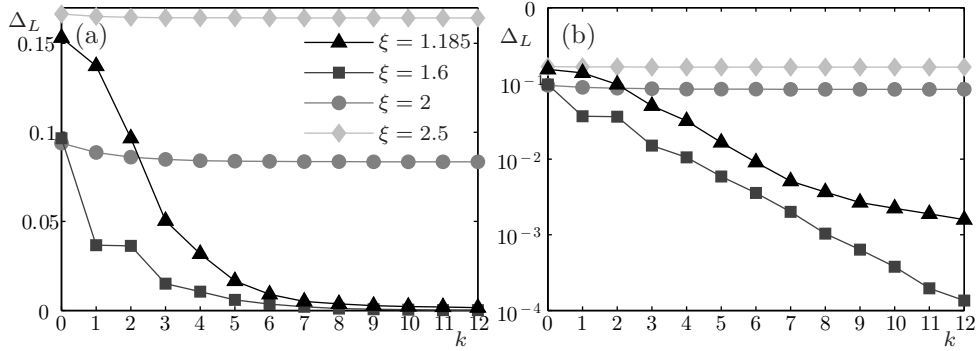


Figure 10: Maximal gap  $\Delta_L$  of  $W_L^s(p^-) \cap \Sigma^+$  for  $\xi \in \{1.185, 1.6, 2.0, 2.5\}$  as a function of  $k$  with  $L = 600 \cdot 2^k$ , shown on a linear  $\Delta_L$ -scale (a) and a logarithmic  $\Delta_L$ -scale (b); here  $\mu = -9.5$  and  $\beta = 0.1$ .

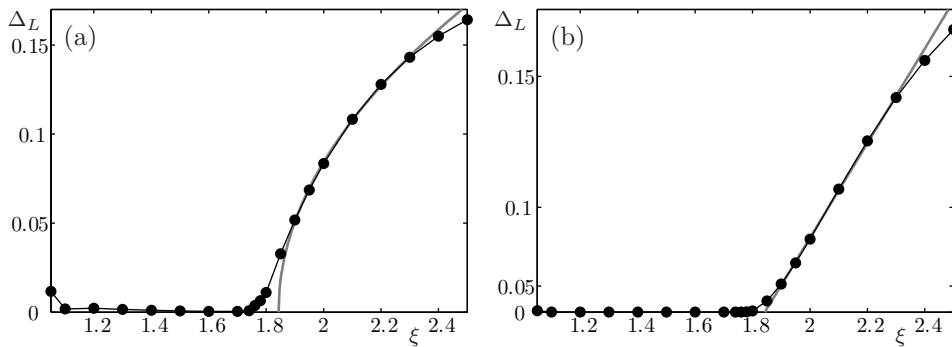


Figure 11: Maximal gap  $\Delta_L$  of  $W_L^s(p^-) \cap \Sigma^+$  for  $L = 600 \cdot 2^{10}$  as a function of  $\xi \in [1.05, 2.5]$  on a linear scale (a) and a quadratic scale (b); here  $\mu = -9.5$  and  $\beta = 0.1$ .

close much more slowly as a function of the arclength  $L$ , and this leads to the larger value of  $\Delta_L$  for  $\xi = 1.05$  in figure 11, because  $L = 600 \cdot 2^{10}$  is fixed.

## 4 The blender for $\xi < 1$

We now investigate the geometry of the blender of the map  $H$  at the parameter values  $\mu = -9.5$ ,  $\beta = 0.1$  for varying  $\xi < 1$ . Recall that for  $\xi < 1$ , the unstable manifold  $W^u(p^-)$  of  $H$  is one dimensional and, therefore, its closure  $\overline{W^u(p^-)}$  forms the unstable manifold of the hyperbolic set  $\Lambda$  of (1), which may be a blender or not. Furthermore, the strong unstable subspace of the inverse  $H^{-1}$  and, hence, the strong stable subspace of  $H$  are nearly parallel to the  $x$ -axis. Therefore, to check that  $W^u(\Lambda)$  has the carpet property, we check whether the projection of  $W^u(p^-)$  onto the  $(\bar{y}, \bar{z})$ -plane is dense in a two-dimensional region. Analogously to our investigation in Section 3, we study the transition of  $W^u(p^-)$  for decreasing values of  $\xi$ , while the arclength  $L$  and the parameters  $\mu = -9.5$  and  $\beta = 0.1$  are kept fixed; moreover, we compute the maximal gap  $\Delta_L$  for varying  $L$  and  $\xi < 1$ .

Figure 12 is the first picture of a blender in the map  $H$  that is formed by an unstable manifold. It shows  $W^u(p^-)$  (orange to red) of  $H$  in  $\mathcal{C}$  computed up to arclength  $L = 3200$ , for  $\mu = -9.5$ ,  $\beta = 0.1$  and  $\xi = 0.9$ . Analogously to the colour scheme of  $W^s(p^-)$  in figure 3, the manifold  $W^u(p^-)$  in figure 12 is coloured orange to red according to the maximal value of  $|\bar{x}|$  for each curve segment starting near the points  $q^\pm$  and ending in the half-plane  $\bar{x} = 0$  for  $\bar{y} > 0$ . Figure 12 (a) shows the bounding circles in  $\partial\mathcal{C}$ , the sinks  $q^\pm$ , the saddle fixed point  $p^-$  and

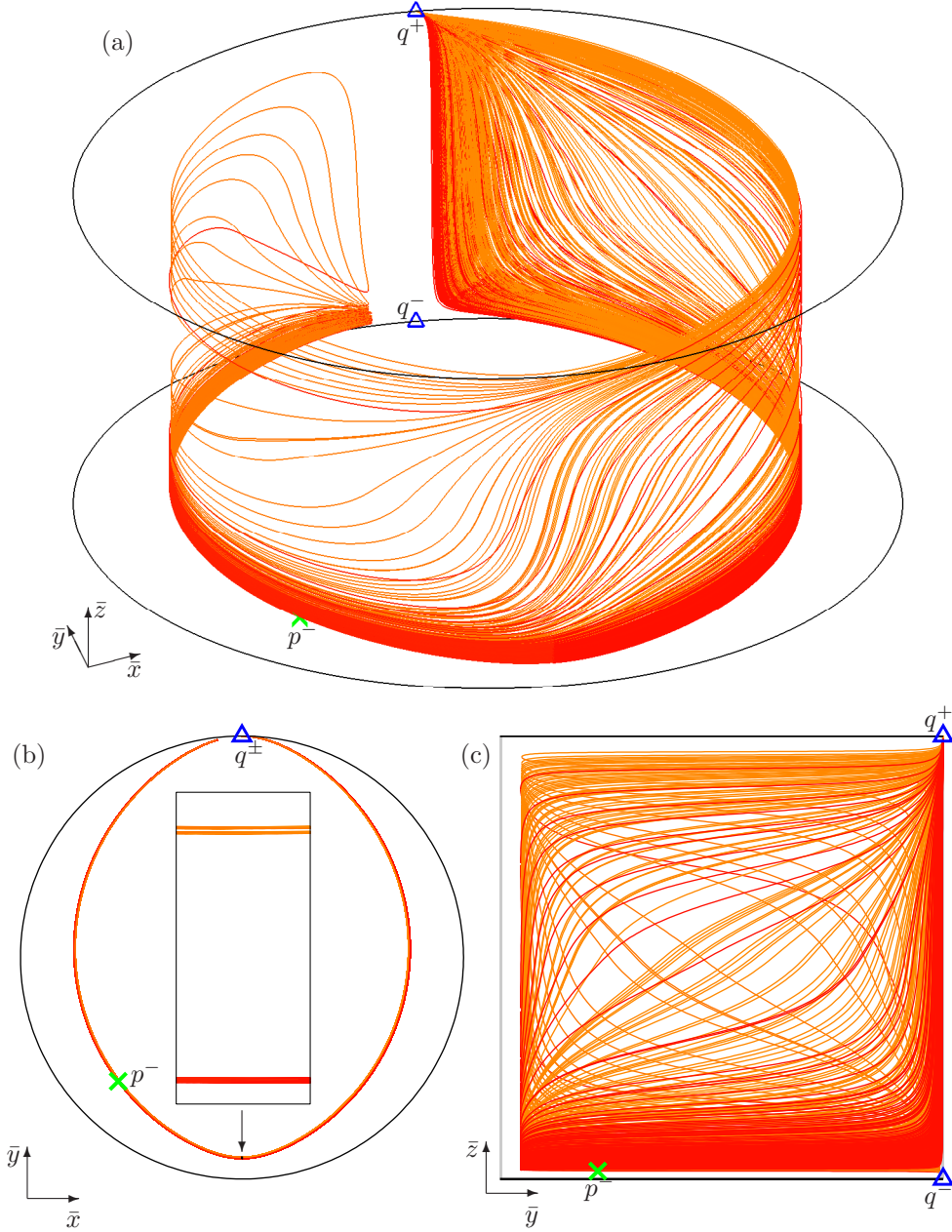


Figure 12: The unstable manifold  $W^u(p^-)$  of  $H$  for  $\xi = 0.9$ , computed up to arclength  $L = 3200$ , shown in  $\mathcal{C}$  (a) and in projections onto  $\mathcal{D}$  (b) and the  $(\bar{y}, \bar{z})$ -plane (c); here  $\mu = -9.5$ ,  $\beta = 0.1$ .

$W^u(p^-)$ . Panel (b) shows the projection onto the disk  $\mathcal{D}$ , reflecting the Cantor-set structure of  $W^u(p^-)$  in the colour scheme; compare with figure 1. Figure 12 (c) shows the projection of  $\mathcal{C}$  in the  $\bar{x}$ -direction onto the  $(\bar{y}, \bar{z})$ -plane  $[-1, 1] \times [-1, 1]$  illustrating the carpet property of  $W^u(p^-)$ . Indeed,  $W^u(p^-)$  appears to be filling up an entire region densely; compare with figure 3(c). Again, computing new segments of  $W^u(p^-)$  for increasing  $L$  brings the overall gap size down. Hence, figure 12 strongly indicates that the closure  $\overline{W^u(p^-)}$  approximates the unstable manifold of a blender of  $H$  for  $\xi = 0.9$ .

Figures 13–15 show the transition of the blender when  $\xi$  is decreased to  $\xi = 0.7$ ,  $0.5$  and  $0.3$ , respectively. Shown are  $W^u(p^-)$  for  $L = 3200$  in  $\mathcal{C}$ , projected onto  $\mathcal{D}$  and projected onto

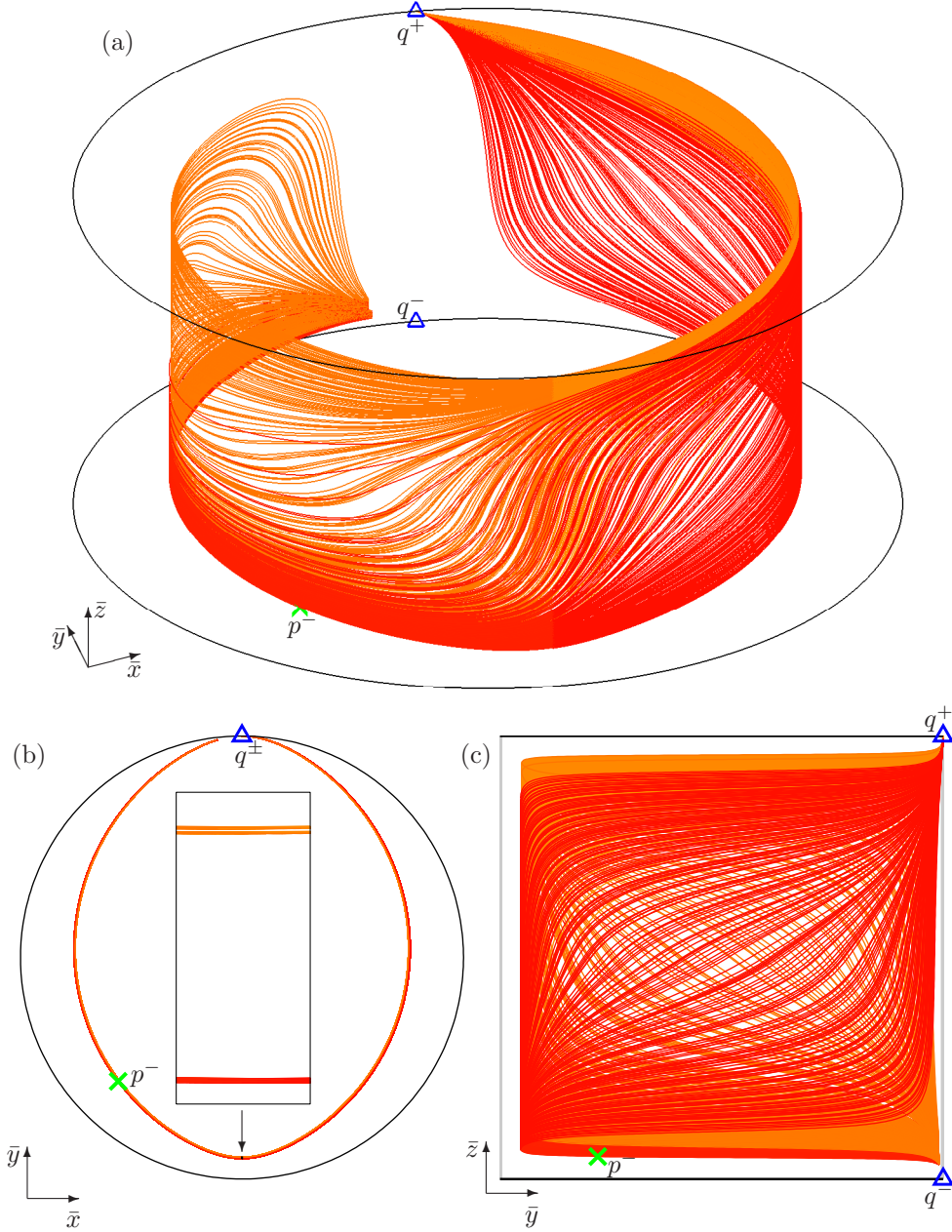


Figure 13: The unstable manifold  $W^u(p^-)$  of  $H$  for  $\xi = 0.7$ , computed up to arclength  $L = 3200$ , shown in  $\mathcal{C}$  (a) and in projections onto  $\mathcal{D}$  (b) and the  $(\bar{y}, \bar{z})$ -plane (c); here  $\mu = -9.5$ ,  $\beta = 0.1$ .

the  $(\bar{y}, \bar{z})$ -plane in panels (a)–(c), respectively. Again, the projections onto  $\mathcal{D}$  do not change, but we observe the following changes in the structure of  $W^u(p^-)$  in panels (a) and (c). The inner (orange) segments and the outer (red) segments of  $W^u(p^-)$  have separated somewhat for  $\xi = 0.7$  in figure 13(a) but their projection in figure 13(c) admits hardly any gaps; compare with figure 7 for  $\xi = 1.6$ . This suggests that  $W^u(p^-)$  still has the carpet property and that  $H$  still has a blender for  $\xi = 0.7$ . Decreasing  $\xi$  to  $\xi = 0.5$  and  $\xi = 0.3$  leads to the inner and outer segments of  $W^u(p^-)$  separating further, such that they span a smaller range of  $\bar{z}$ -values. More importantly, we now find obvious gaps in projection onto the  $(\bar{y}, \bar{z})$ -plane; see figure 14(a) and (c) and figure 15(a) and (c), respectively. As in figures 8 and 9 for  $\xi = 2$  and  $\xi = 2.5$ ,

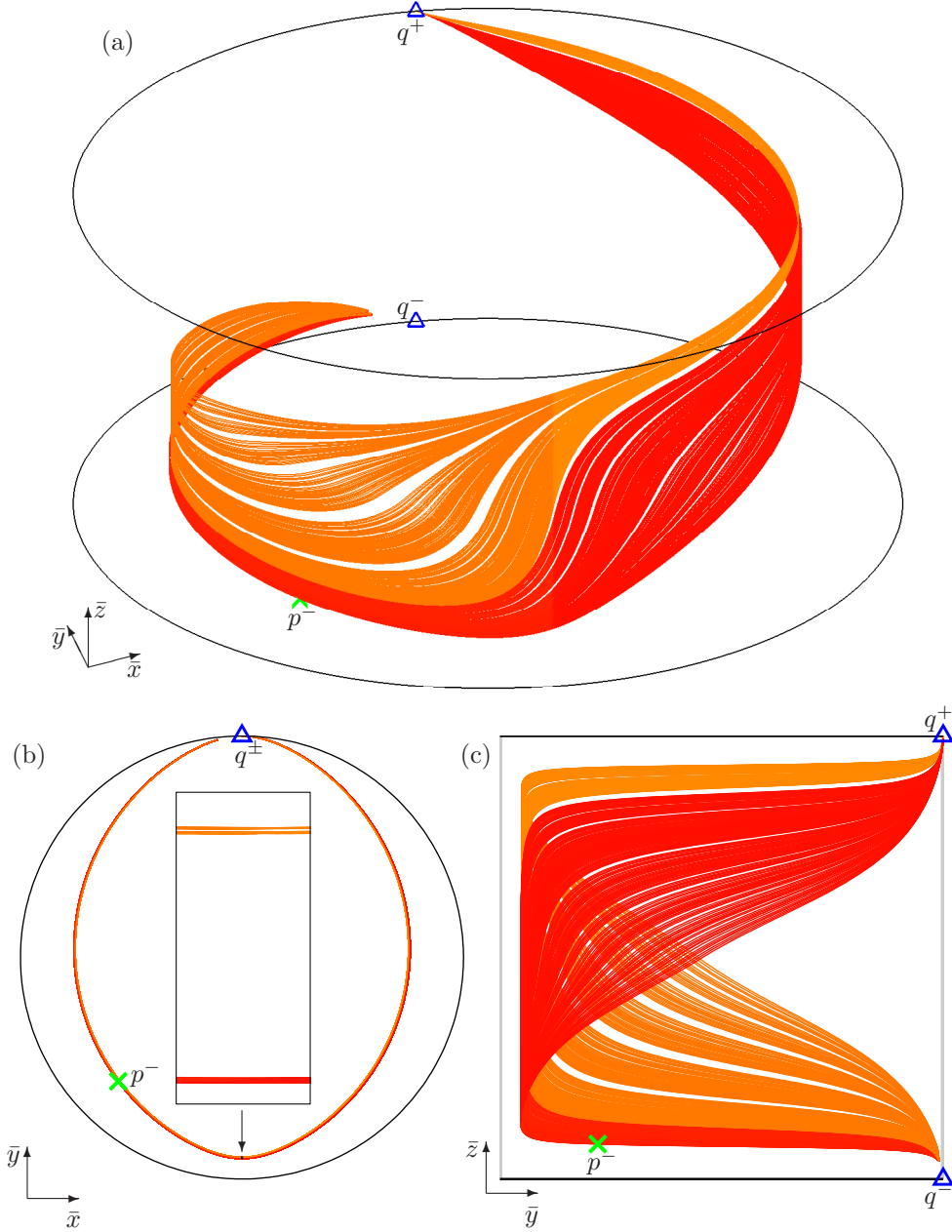


Figure 14: The unstable manifold  $W^u(p^-)$  of  $H$  for  $\xi = 0.5$ , computed up to arclength  $L = 3200$ , shown in  $\mathcal{C}$  (a) and in projections onto  $\mathcal{D}$  (b) and the  $(\bar{y}, \bar{z})$ -plane (c); here  $\mu = -9.5$ ,  $\beta = 0.1$ .

respectively, these gaps appear to be distributed over the range of  $\bar{z}$ -values in a Cantor-set structure and, when computing  $W^u(p^-)$  for increasing  $L$ , the visible gaps do not decrease for  $\xi = 0.5$  and  $\xi = 0.3$ . Therefore, figures 14 and 15 suggest that  $W^u(p^-)$  no longer has the carpet property and that  $H$  no longer has a blender for  $\xi = 0.5$  and  $\xi = 0.3$ . Hence, figures 13–15 are numerical evidence that  $W^u(p^-)$  initially still has the carpet property and a blender exists when  $\xi$  is decreased from  $\xi = 1$ , but that the carpet property is lost when  $\xi$  becomes too small.

Analogously to our computations of the maximal gap  $\Delta_L$  of  $W^s(p^-)$  in section 3.2, we adapt our method to compute the maximal gap  $\Delta_L$  of  $W^u(p^-)$  as follows. We intersect  $W^u(p^-)$  with the plane  $\Sigma^+ := \{(\bar{x}, \bar{y}, \bar{z}) : \bar{y} = 0, \bar{y} > 0\}$ , order the  $N_L$  intersection points up to arclength  $L$

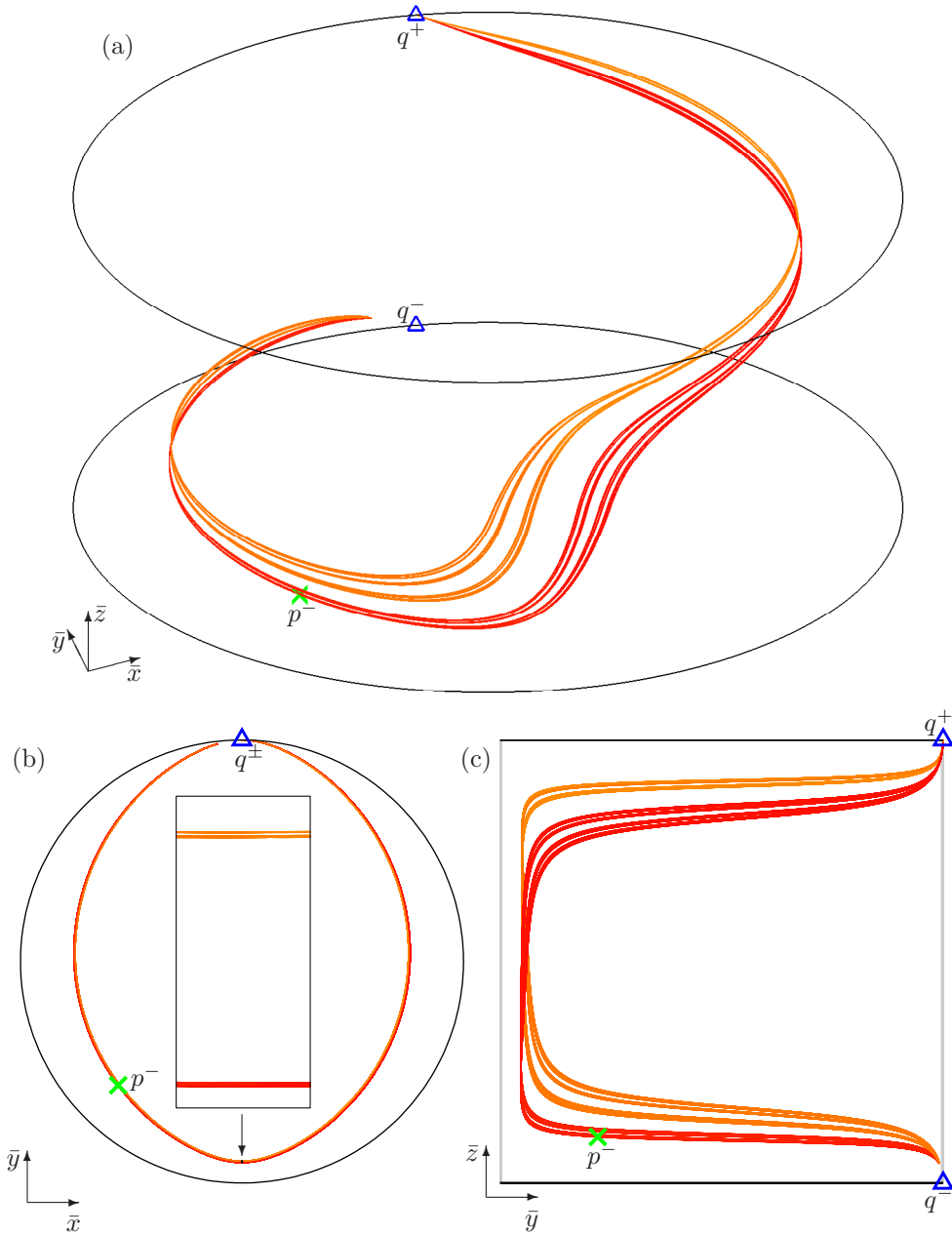


Figure 15: The unstable manifold  $W^u(p^-)$  of  $H$  for  $\xi = 0.3$ , computed up to arclength  $L = 3200$ , shown in  $\mathcal{C}$  (a) and in projections onto  $\mathcal{D}$  (b) and the  $(\bar{y}, \bar{z})$ -plane (c); here  $\mu = -9.5$ ,  $\beta = 0.1$ .

by increasing values of  $\bar{z}$  and define the maximal gap for the projection in the  $\bar{x}$ -direction as in (8). Note that the only difference to the maximal gap  $\Delta_L$  as computed in Section 3.2 is that we intersect with the plane  $\{\bar{y} = 0\}$  instead of  $\{\bar{x} = 0\}$  to reflect the change to projection along the  $\bar{y}$ -axis, which is nearly parallel to the strong stable subspace of  $H$ . We initially consider  $L = 400 \cdot 2^k$ , for which we find  $N_L \approx 32 \cdot 2^k$  for  $\xi = 0.9$ .

Figure 16 presents more substantial numerical evidence for the existence or non-existence of the blender for  $\xi < 1$ . Namely, panels (a) and (b) show the maximal gap  $\Delta_L$  of  $W_L^u(p^-)$  as a function of  $k \in \{0, \dots, 12\}$  with  $L = 400 \cdot 2^k$  for  $\xi = 0.9$  (triangles),  $\xi = 0.7$  (squares),  $\xi = 0.5$  (circles) and  $\xi = 0.3$  (diamonds) on a linear and logarithmic scale, respectively; compare with

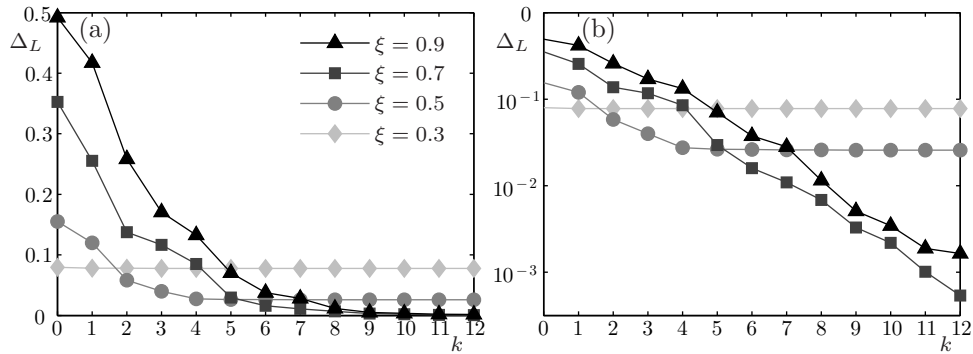


Figure 16: Maximal gap  $\Delta_L$  of  $\bar{z}$ -coordinates in  $W_L^u(p^-) \cap \Sigma^+$  over  $k$  with  $L = 200 \cdot 2^k$  for  $\xi \in \{0.3, 0.5, 0.7, 0.9\}$  on a linear scale (a) and a logarithmic scale (b).

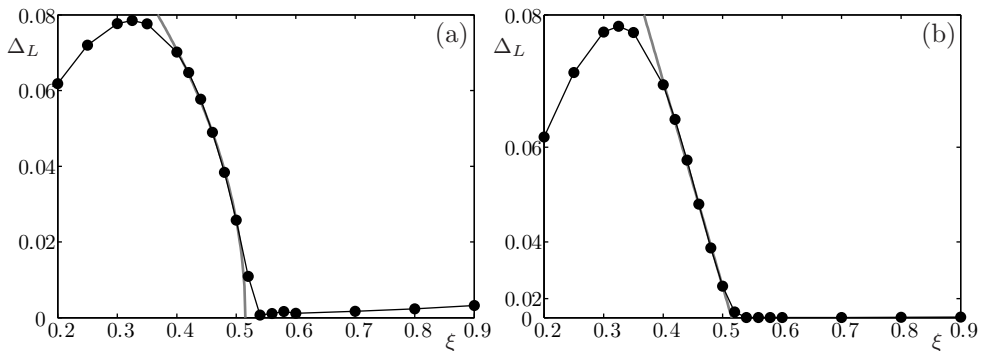


Figure 17: Maximal gap  $\Delta_L$  of  $W_L^u(p^-) \cap \Sigma^+$  for  $L = 200 \cdot 2^{10}$  as a function of  $\xi \in [0.2, 0.9]$  on a linear scale (a) and a quadratic scale (b); here  $\mu = -9.5$  and  $\beta = 0.1$ .

figure 10. We notice in figure 16 that  $\Delta_L$  decays exponentially for  $\xi = 0.9$  and  $\xi = 0.7$  and that it converges rapidly to fixed positive values  $\Delta_L \approx 0.0257$  and  $\Delta_L \approx 0.0777$  for  $\xi = 0.5$  and  $\xi = 0.3$ , respectively. This confirms our initial observations that  $W^u(p^-)$  has the carpet property for  $\xi = 0.9$  and  $\xi = 0.7$ , but not for  $\xi = 0.5$  and  $\xi = 0.3$ .

As in figure 10, we notice only little change in  $\Delta_L$  for  $k \geq 10$  in figure 16. Hence, we fix  $L = 200 \cdot 2^{10}$  in figure 17(a) and (b), where the maximal gap  $\Delta_L$  is shown as a function of  $\xi \in [0.2, 0.9]$  on a linear and a quadratic scale, respectively; compare with figure 11. We observe that  $\Delta_L$  is very small and, in fact, decreasing to about  $10^{-4}$  for decreasing  $\xi \in [0.54, 0.9]$ . It then increases considerably for  $\xi < 0.54$  in an approximately square-root fashion. Correspondingly, the plot on the quadratic scale is practically linear for  $\xi \leq 0.54$  and we compute the least squares regression line (grey) for the data points at  $\xi \in \{0.4, 0.42, 0.44, 0.46, 0.48, 0.5\}$  on the quadratic scale in panel (b), which corresponds to a square-root curve (grey) on the linear scale in panel (a). Analogously to our analysis of the maximal gap  $\Delta_L$  of  $W^s(p^-)$  for  $\xi > 1$ , we estimate that the carpet property is lost and the blender is destroyed near the value  $\xi^{**} := 0.515$ , where the regression line (and, hence, the square-root curve) crosses zero.

## 5 Conclusions and outlook

To investigate the geometry of blenders in the three-dimensional Hénon-like family  $H$  of diffeomorphisms (1), we introduced a numerical method or test whether the key property of a blender is satisfied. More specifically, we test for what we call the carpet property, which boils down to checking that a one-dimensional stable or unstable manifold fills up an area densely

in a suitable projection. To achieve this, we compute the respective one-dimensional manifold as a curve, parametrized by arclength, in the compactified phase space. This compactification is important because it controls the growth of the arclength of the curve during excursions to points near infinity. This type of manifold computation is used in two ways: (1) to generate images of blenders in the compactified phase space, and (2) to determine the maximal gap size in the projection as a function of arclength. In this way, we are able to illustrate the geometry of manifold structure, while the decay of the gap size with arclength provide strong evidence for whether or not the manifold has the carpet property. This approach was also used to demonstrate robustness with respect to the projection angle.

We demonstrated that these computational tools are able to provide convincing evidence for when a blender exists in the three-dimensional Hénon-like family  $H$  for the case that the Hénon map has a full horseshoe. Moreover, they allowed us to produce the first images of what a blender looks like by means of showing the associated manifolds structure. In this study we varied the parameter  $\xi$ , which is the eigenvalue of the third, new and shear-like direction. Previous work in [11] for a related but different Hénon-like map suggested that  $H$  should have a blender for  $\xi = 1.185$ . This was indeed confirmed by computations of the one-dimensional stable manifold  $W^s(p^-)$  of a saddle fixed point  $p^-$ , and the convergence to zero of the associated maximal gap with arclength of the computed part of  $W^s(p^-)$ . We proceeded by considering increasing values of  $\xi$  and found that  $W^s(p^-)$  loses the carpet property and, hence,  $H$  no longer has a blender, for  $\xi^* \approx 1.843$ . For  $\xi > 1.843$  we find that the projection of  $W^s(p^-)$  appears to have the (local) structure of a Cantor set of curves. We performed a similar analysis for  $\xi < 1$ , when the blender is associated to the unstable manifold  $W^u(p^-)$ . Analogously, we found that  $W^u(p^-)$  has the carpet property close to  $\xi = 1$  until down to about  $\xi^{**} \approx 0.515$ , after which  $W^u(p^-)$  now appears to have the (local) structure of a Cantor set of curves.

Overall, we presented evidence that  $H$  has a blender for quite a large interval of  $\xi$ -values around  $\xi = 1$ . This is interesting because theory requires that the attraction or repulsion associated with  $\xi$  be sufficiently small (as it is the centre direction). Moreover, we observed the destruction or creation of a blender. The results are observations based on a careful study with advanced numerical techniques. Mathematically speaking, they have the status of a conjecture that, we hope, will stimulate further development of the theory and new techniques of proof.

An obvious first task is to prove that  $H$  indeed has a blender. This can be achieved by considering a single, suitable point in parameter space. A good choice is  $\mu = -9.5$ ,  $\beta = 0.1$  and  $\xi = 1.185$ , which is motivated by the parameter values for which the existence of a blender was proved in the nearby map (3) from [11]. The difference is that the map (3) is an endomorphism (that is, noninvertible) and not a diffeomorphism. Nevertheless, motivated by our numerical results and the approach taken in [11], we constructed the proof for  $H$  at the above parameter values. It is important to realize that the method of proof is entirely complimentary to the numerical approach taken to show the carpet property. Namely, the proof requires one to show that a certain region of phase space, a box, returns to itself subject to satisfying certain estimates for cone fields associated with the stable, centre and unstable directions. The required properties can be verified in a number of steps that require certain estimates to hold. More specifically, the main proposition that is equivalent to the carpet property requires verifying five conditions about the position of the image of the box, about the invariance and hyperbolicity of the three cone fields, and about how certain segments return to the box; the technical statement and the full proof can be found in Appendix A.

We remark that the estimates and, hence, the proof hold in some small neighbourhood around the chosen parameter point. It is a different task to prove the blender property throughout the entire interval that our study suggests. One would certainly expect that it

will become more difficult to verify the blender property in the same way when the boundaries of the interval of its existence are approached. Moreover, this method of proof cannot be used to make a statement about when and how the blender property is lost. In future work, we intend to investigate the details of this new type of global bifurcation, that is, the mechanism by which the carpet property is lost. This will entail, in the first instance, the characterization of the properties of the global one-dimensional manifolds after the blender disappears, as well as a study of how the bifurcation loci change as the other parameters of  $H$  are varied. We hope that such an investigation will provide further geometric insight that may contribute to a bifurcation theory of blenders.

In this context we mention that the map  $H$  does not admit hyperbolic sets with other indices than those of the blenders or the fixed points and, therefore, it cannot admit heterodimensional cycles. It is an interesting question whether one can perturb this map in such a way that it allows for the existence of hyperbolic sets of other indices. In particular, we are interested in the question of whether one could create heterodimensional cycles involving the blenders of the map  $H$  and study their robustness. Another line of future research is to apply our methods for the investigation of other explicit systems that admit blenders or heterodimensional cycles. One explicit example of a two-dimensional endomorphism with a “solenoidal blender” is given in [2]. Another interesting (but semi-explicit) example is the family of three-dimensional Hénon-like diffeomorphism studied in [13, 14].

## 5.1 Blender-like attractors

We finish this paper with an outlook regarding attractors with the carpet property. These may arise naturally from certain global bifurcations of blenders, such as boundary crisis bifurcations where hyperbolic sets bifurcate to create chaotic attractors. In ongoing work in this direction we are studying the map  $H$  for the classical parameter regime  $\mu = -1.4$  and  $\beta = 0.3$  of the Hénon map (2), when its nonwandering set  $\Lambda_h$  of (2) no longer forms a full horseshoe but a *pruned horseshoe* (meaning that some symbolic sequences are missing [9]) and one finds the well-known chaotic Hénon attractor.

Figure 18 illustrates the classical (compactified) Hénon map on the disk  $\mathcal{D}$ ; compare with figure 1. Since the homoclinic tangle now forms a pruned horseshoe, the involved manifolds locally still form Cantor-set structures, but some segments of  $W^u(p_h^\pm)$  intersect segments of  $W^s(p_h^\pm)$  only twice or not at all. This means that an infinite sequence of homoclinic and heteroclinic orbits has disappeared in an infinite sequence of homoclinic and heteroclinic tangencies between  $W^u(p_h^\pm)$  and  $W^s(p_h^\pm)$  that occurred during the transition from  $(\mu, \beta) = (-9.5, 0.1)$  to  $(\mu, \beta) = (-1.4, 0.3)$ ; for details on the Hénon map, see, for example, [27]. Moreover, for  $(\mu, \beta) = (-1.4, 0.3)$ , the unstable manifold  $W^u(p_h^-)$  is bounded by the outer segments of the stable manifold  $W^s(p_h^+)$  and its closure  $\overline{W^u(p_h^-)}$  forms the chaotic Hénon attractor. Indeed, the basin of this attractor is bounded by  $W^s(p_h^+)$ . Hence, one side of  $W^u(p_h^+)$  still goes to infinity while the other side goes to the chaotic attractor. In particular, the closure  $\overline{W^u(p_h^-)}$  is contained in  $\overline{W^u(p_h^+)}$ , but they no longer coincide.

When considering the three-dimensional map  $H$  for  $\mu = -1.4$  and  $\beta = 0.3$ , the closure  $\overline{W^u(p^-)}$  forms an attractor for  $\xi < 1$ . It is a natural question to ask whether the one-dimensional manifold  $W^u(p^-)$  still has the carpet property. Figure 19 is the first picture of such a blender-like attractor of the map  $H$ ; compare with Figures 12–15 for  $(\mu, \beta) = (-9.5, 0.1)$ . Panel (b) shows that the projection onto  $\mathcal{D}$  is, indeed, simply the Hénon attractor represented by  $W^u(p^-)$ . The projection onto the  $(\bar{y}, \bar{z})$ -plane, on the other hand, suggests that  $W^u(p^-)$  may still have the carpet property. The difference is now that this appears to happen along some strips, rather than over a large and quite uniform area. To check this we compute the maximal gap  $\Delta_L$  locally in a small strip above the fixed point  $p^-$  by considering intersections of

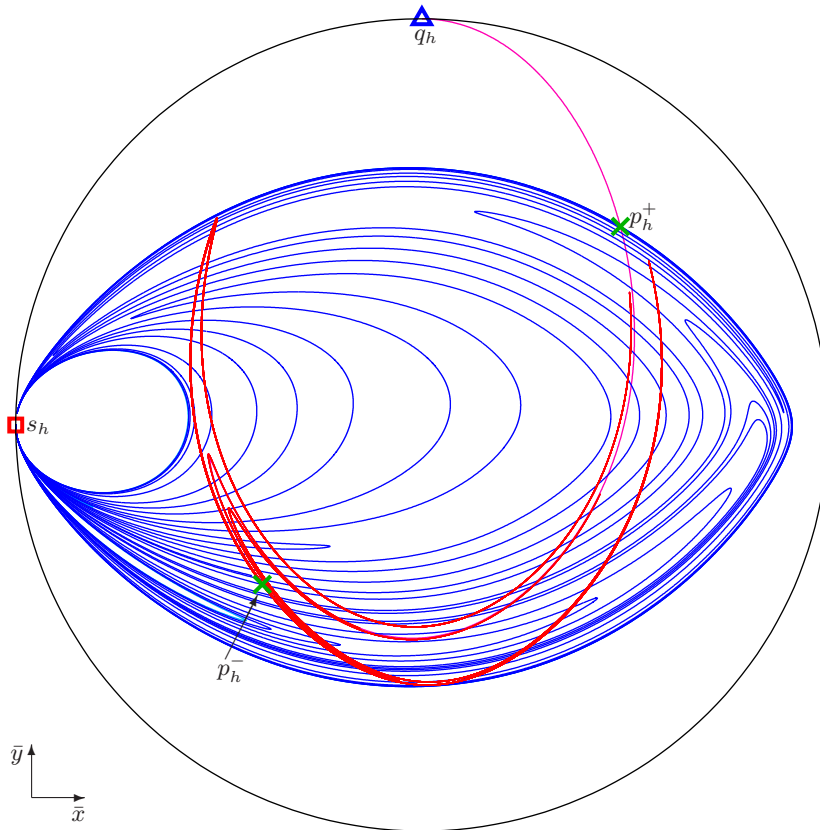


Figure 18: The two-dimensional Hénon map (2) for  $\mu = -1.4$  and  $\beta = 0.3$  on the Poincaré disk  $\mathcal{D}$ . Shown are  $\partial\mathcal{D}$  (black unit circle), the sink  $q_h \in \partial\mathcal{D}$  (blue triangle), the source  $s_h \in \partial\mathcal{D}$  (red square), the saddle fixed points  $p_h^+$  and  $p_h^-$  (green crosses), and their stable and unstable manifolds  $W^s(p_h^\pm)$  (blue and cyan) and  $W^u(p_h^\pm)$  (red and magenta), computed up to arclength  $L = 100$ .

$W_L^u(p^-)$  only with the subset  $\Sigma_z^+ := \{(\bar{x}, 0, \bar{z}) : \bar{x} > 0, \bar{z} \in [\bar{p}_z^-, \bar{p}_z^- + 0.1]\}$ , where  $\bar{p}_z^- \approx -0.48565$  is the  $\bar{z}$ -coordinate of  $p^-$ . Note that, since the non-wandering set forms a pruned horseshoe instead of a full horseshoe and we only consider the subregion  $\Sigma_z^+$ , the arclength  $L$  and the number  $N_L$  of points in  $W_L^u(p^-) \cap \Sigma_z^+$  are no longer directly proportional. Figure 20 shows  $\Delta_L$  (restricted to  $\Sigma_z^+$ ) as a function of  $k$  for  $L = 200 \cdot 2^k$ , on a linear scale in panel (a) and on a logarithmic scale in panel (b).

The observed exponential convergence of  $\Delta_L$  to zero strongly suggests that the attractor of  $H$  in figure 19 has the carpet property and, hence, can be called a blender-like attractor. Further study will concentrate on the properties of this object and how it emerges and bifurcates as the central eigenvalue  $\xi$  as well as the parameters  $\mu$  and  $\beta$  of the Hénon map are varied.

## Acknowledgements

We thank Andy Hammerlindl and Gemma Mason for helpful discussions. BK and HMO were supported by Royal Society of New Zealand Marsden Fund grant 16-UOA-286. KS was supported by JSPS KAKENHI grant 16K17609.

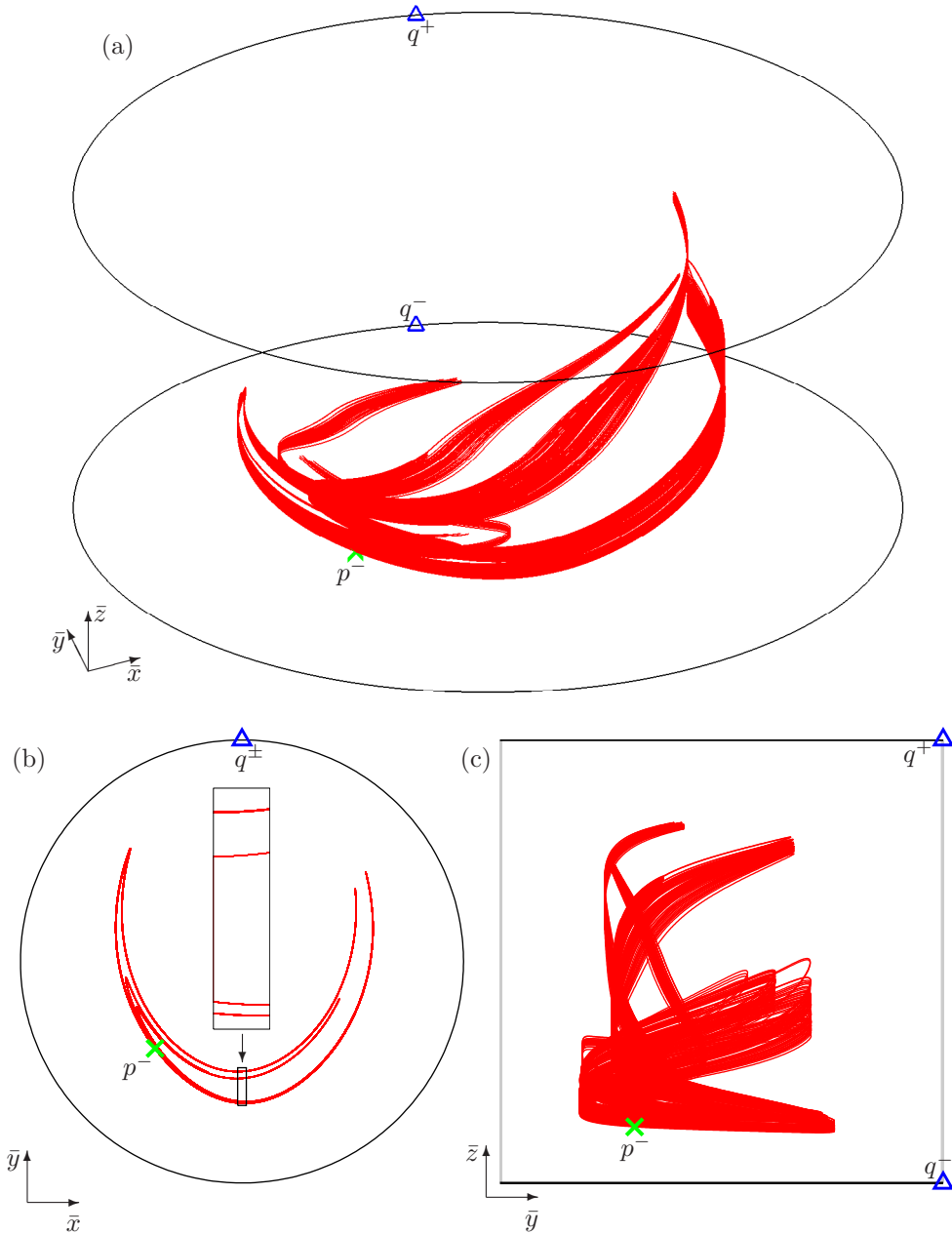


Figure 19: The unstable manifold  $W^u(p^-)$  of  $H$  for  $\mu = -1.4$ ,  $\beta = 0.3$ , and  $\xi = 0.7$ , computed up to arclength  $L = 3200$ , shown in  $\mathcal{C}$  (a) and in projections onto  $\mathcal{D}$  (b) and the  $(\bar{y}, \bar{z})$ -plane (c).

## Appendix A Computation of one-dimensional manifolds

We now explain how we compute the one-dimensional manifolds in this paper as long curves in the compactified phase space  $\mathcal{C}$ . To be specific, we consider the computation of  $W^u(p)$  of a fixed point  $p \in \mathcal{C}$  of the map  $H$  acting on  $\mathcal{C}$ ; a one-dimensional stable manifold can be computed analogously as the unstable manifold of the inverse  $H^{-1}$ . Our overall computational method is based on the algorithm from [19], which grows (one side of) a one-dimensional manifold point by point until a specified arclength is reached. We use its implementation in the DS`TOOL` environment [1, 12, 18] to compute an initial large piece of arclength  $L$ . We then import this manifold data from DS`TOOL` into `MATLAB`, where it is used to render images and

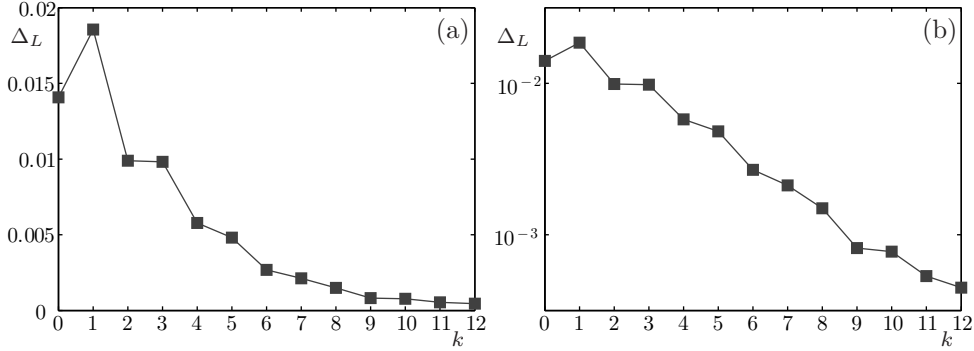


Figure 20: Maximal gap  $\Delta_L$  of  $\bar{z}$ -coordinates in  $W_L^u(p^-) \cap \Sigma_z^+$  over  $k$  with  $N = N_0 \cdot 2^k$  for  $\xi = 0.7$  on a linear scale (a) and a logarithmic scale (b).

to determine the maximal gap  $\Delta_L$  as a function of doubling  $L$  repeatedly. To achieve the latter efficiently, we use an adapted version of the same algorithm and double the arclength step by step; performing these doubling steps in MATLAB is much more efficient, because it avoids transferring very large amounts of data from the stand-alone package DSTOOL; recall that we compute one-dimensional manifolds and  $\Delta_L$  for arclengths up to  $L = 600 \cdot 2^{12}$ .

The underlying idea of the growth algorithm from [19] is the following. The approximation of  $W^u(p)$  is represented at step  $k$  of the computation by  $\text{Lin}(p, z_1, \dots, z_k)$ , consisting of line segments between consecutive points  $p, z_1, \dots, z_k$  with  $z_i \in \mathcal{C}$  for  $1 \leq i \leq k$ ; here, the point  $z_1$  is in the unstable eigenspace of  $p$  at some small distance  $\delta_0$  from  $p$ . We then compute a candidate for the next point  $z_{k+1}$  at distance  $\delta_k$  from  $z_k$  such that  $z_{k+1} = H(z)$  for some  $z \in \text{Lin}(p, z_1, \dots, z_k)$ . To ensure an appropriate representation of the manifold where  $W^u(p)$  has large curvature, we accept the candidate  $z_{k+1}$  only if the angle  $\alpha_k \in [0, \pi]$  between the vectors  $z_k - z_{k-1}$  and  $z_{k+1} - z_k$  is not too large. Moreover,  $\delta_k$  can be chosen larger if  $\alpha_k$  is relatively small, that is, we also monitor the product  $\delta_k \alpha_k$ . In this way, the point distribution is adapted to the curvature according to prespecified accuracy parameters; see [19] for details. The computation stops when the given arclength  $L$  is reached, that is, when  $\sum_{k=0}^N \delta_k \approx L$ . We then proceed by computing the intersection points of  $\text{Lin}(p, z_1, \dots, z_N)$  with the plane  $\Sigma$ , which are ordered to determine the maximal gap  $\Delta_L$  or  $\Delta_L^\alpha$ , as described in section 3.2.

The key idea behind the growth method is that the approximation satisfies prespecified accuracy conditions at every stage; in particular, any interpolation is performed with a controlled accuracy due to the curvature adaption. This means that the numerical approximation of  $W^u(p)$  and its intersection with  $\Sigma$  can be computed as accurately as required. The technical statement is that the computed manifold up to arclength  $L$  lies in an  $\varepsilon$ -neighbourhood of  $W^u(p)$  in the Hausdorff metric, provided the accuracy parameters are chosen stringent enough; we refer to [19, 20] for more details.

## Appendix B Proof of the existence of a blender in the map $H$

In section 3, we numerically investigated the map  $H$ , given by (1) for  $\mu = -9.5$ ,  $\beta = 0.1$  and  $\xi > 0$ , and observed the carpet property of the stable manifold  $W^s(p^-)$  of the saddle fixed point  $p^-$  for a range of  $\xi$ -values that included  $\xi = 1.185$ . In this section, we prove that this diffeomorphism of  $\mathbb{R}^3$  does, indeed, have a blender for  $\mu = -9.5$ ,  $\beta = 0.1$  and  $\xi = 1.185$ . More precisely, we prove that the stable manifold  $W^s(p^+)$  of the other saddle fixed point  $p^+$  contained in the hyperbolic set  $\Lambda$  has the carpet property; namely, every curve segment in a certain direction and a certain region of phase space intersects  $\overline{W^s(p^+)}$ ; we use  $W^s(p^+)$  instead

of  $W^s(p^-)$  in order to follow the proof from [11] for the perturbed map (3) more closely. Recall that both  $W^s(p^-)$  and  $W^s(p^+)$  are dense in  $W^s(\Lambda)$ , so either manifold can be used to show the carpet property of  $W^s(\Lambda)$ . Also, note that, in line with [11], we use the notation  $\mathcal{C}$  to represent a cone field; in this section  $\mathcal{C}$  does not refer to the compactified phase space.

## B.1 Background and statement

To state the result, we introduce some notation. We define the box

$$\mathcal{R} := [-4, 4] \times [-4, 4] \times [-40, 0] \subset \mathbb{R}^3.$$

Inside this region we have the unique hyperbolic fixed point  $p^+ = (x^+, y^+, z^+)$  of stable index one. As we observed in section 2.2 (see also B.2), the coordinates of this point are approximately  $(3.565, 3.565, -14.404)$ .

For  $p \in \mathbb{R}^3$ , we identify  $T_p\mathbb{R}^3$  with  $\mathbb{R}^3$  with respect to the basis  $\langle \partial_x, \partial_y, \partial_z \rangle$  and we write  $v = (s, t, u)$  for  $v \in T_p\mathbb{R}^3$ . We introduce three cone fields over  $\mathcal{R}$ : we define the *centre unstable cone field*

$$\mathcal{C}^u(p) := \left\{ (s, t, u) \mid 2|s| \leq \sqrt{t^2 + u^2} \right\},$$

the *strong unstable cone field*

$$\mathcal{C}^{uu}(p) := \left\{ (s, t, u) \mid 2\sqrt{s^2 + u^2} \leq |t| \right\},$$

and the *stable cone field*

$$\mathcal{C}^s(p) := \left\{ (s, t, u) \mid 2\sqrt{t^2 + u^2} \leq |s| \right\},$$

with principal axes approximately equal to the corresponding (strong) unstable and stable eigenvectors of  $p^+$ . As we will see later,  $\mathcal{C}^u$  and  $\mathcal{C}^{uu}$  are forward invariant and  $\mathcal{C}^s$  is backward invariant.

By a *segment* we mean a  $C^1$ -embedding  $\sigma : I \rightarrow \mathcal{R}$ . We say that a segment  $\sigma$  is *tangent to a cone field  $\mathcal{C}$*  if  $T\sigma \subset \mathcal{C}$  holds at every point in the image of  $\sigma$ . By  $W_0^s(p^+)$  we denote the connected component of  $W^s(p^+) \cap \mathcal{R}$  that contains  $p^+$ . We later observe that  $W_0^s(p^+)$  is tangent to  $\mathcal{C}^s$ .

A *vertical segment* is a segment that is tangent to  $\mathcal{C}^{uu}$  and has its end points in  $\partial^{uu}\mathcal{R} := [-4, 4] \times \{-4, 4\} \times [-40, 0]$ . One can check that the set of vertical segments that are disjoint from  $W_0^s(p^+)$  has two homotopy classes. We refer to the one that contains the vertical segments in  $\partial^{u^+}\mathcal{R} := [-4, 4] \times [-4, 4] \times \{0\}$  as *to the right of  $W_0^s(p^+)$*  and call the other one *to the left of  $W_0^s(p^+)$* . Let  $W_{\text{loc}}^s(p^+)$  be defined as in Section 2.4.

Now we are ready to state the main result.

**Proposition 1** *For the map  $H$  with  $\mu = -9.5$ ,  $\beta = 0.1$  and  $\xi = 1.185$ , every vertical segment to the right of  $W_0^s(p^+)$  has non-empty intersection with  $\overline{W_{\text{loc}}^s(p^+)}$ .*

Proposition 1 implies that the stable manifold of  $p^+$  has the carpet property in the region  $\{(x, z) \mid -4 < x < 4 \text{ and } -19 \leq z \leq 0\}$  (in the uncompactified coordinates of  $\mathbb{R}^3$ ). It follows that the underlying hyperbolic set  $\Lambda$  is a (conceptual) blender of  $H$  in the sense of section 2.

We prove Proposition 1 by verifying five conditions, (H1)–(H5) defined below, about the position of the image  $H(\mathcal{R}) \cap \mathcal{R}$ , about the invariance and hyperbolicity of the cone fields  $\mathcal{C}^u$ ,  $\mathcal{C}^{uu}$  and  $\mathcal{C}^s$ , and about the position of the vertical segments to the right of  $W_0^s(p^+)$  with respect to  $W_0^s(p^-)$  and the left and right boundaries of  $\mathcal{R}$ ; see [11, 5]. In what follows, we will use that  $\mu = -9.5$ ,  $\beta = 0.1$  and  $\xi = 1.185$ .

To state the five conditions, we define the subsets of the boundary  $\partial\mathcal{R}$  of  $\mathcal{R}$  as

$$\partial^{uu}\mathcal{R} := [-4, 4] \times \{-4, 4\} \times [-40, 0],$$

$$\partial^s\mathcal{R} := \{-4, 4\} \times [-4, 4] \times [-40, 0],$$

and

$$\partial^u\mathcal{R} := \partial^{u^+}\mathcal{R} \cup \partial^{u^-}\mathcal{R},$$

where

$$\partial^{u^+}\mathcal{R} := [-4, 4] \times [-4, 4] \times \{0\}$$

and

$$\partial^{u^-}\mathcal{R} := [-4, 4] \times [-4, 4] \times \{-40\}.$$

Indeed, locally there is uniform hyperbolicity on  $\mathcal{R}$ , and  $\partial^s\mathcal{R}$ ,  $\partial^u\mathcal{R}$  and  $\partial^{uu}\mathcal{R}$  correspond to the stable, centre unstable and strong unstable directions on  $\mathcal{R}$ .

Finally, we introduce a norm  $\|\cdot\|_0$  on  $T\mathbb{R}^3$  as follows:

$$\|(s, t, u)\|_0 = \max\left\{|s|, \sqrt{t^2 + u^2}\right\}.$$

Now, we are ready to state the five conditions:

- (H1) There is a connected component  $A^+$  of  $\mathcal{R} \cap H(\mathcal{R})$  that is disjoint from  $\partial^s\mathcal{R}$  and  $H(\partial^u\mathcal{R})$ .
- (H2) There is a connected component  $A^-$  of  $\mathcal{R} \cap H(\mathcal{R})$  that is disjoint from  $\partial^s\mathcal{R}$ ,  $\partial^{u^+}\mathcal{R}$  and  $H(\partial^{uu}\mathcal{R})$ .
- (H3) Invariance and hyperbolicity of the cone fields  $\mathcal{C}^u$ ,  $\mathcal{C}^{uu}$  and  $\mathcal{C}^s$ , namely:
  - (i)  $\mathcal{C}^u$  is strictly forward invariant and uniformly expanding on  $\mathcal{R}$ . Namely, for every  $p \in H^{-1}(A^+ \cup A^-)$  and for every  $v \in \mathcal{C}^u(p) \setminus \{(0, 0, 0)\}$ , we have  $D_p H(v) \in \text{int}(\mathcal{C}^u(H(p)))$  and  $\|(D_p H)(v)\|_0 > \|v\|_0$ .
  - (ii)  $\mathcal{C}^{uu}$  is strictly forward invariant and uniformly expanding on  $\mathcal{R}$ . Namely, for every  $p \in H^{-1}(A^+ \cup A^-)$  and for every  $v \in \mathcal{C}^{uu}(p) \setminus \{(0, 0, 0)\}$ , we have  $D_p H(v) \in \text{int}(\mathcal{C}^{uu}(H(p)))$  and  $\|(D_p H)(v)\|_0 > \|v\|_0$ .
  - (iii)  $\mathcal{C}^s$  is strictly backward invariant and uniformly contracting on  $\mathcal{R}$ . Namely, for every  $p \in A^+ \cup A^-$  and for every  $v \in \mathcal{C}^s(p) \setminus \{(0, 0, 0)\}$ , we have  $(D_p H^{-1})(v) \in \text{int}(\mathcal{C}^s(H^{-1}(p)))$  and  $\|(D_p H^{-1})(v)\|_0 > \|v\|_0$ .
- (H4) There is a neighbourhood  $U^-$  of  $\partial^{u^-}\mathcal{R}$  such that every vertical segment to the right of  $W_0^s(p^+)$  has no intersection with  $U^-$ .
- (H5) There exist a neighbourhood  $U$  of  $W_0^s(p^+)$  and  $U^+$  of  $\partial^{u^+}\mathcal{R}$  such that for every vertical segment  $\sigma$  that is to the right of  $W_0^s(p^+)$ , one of the following conditions holds:
  - (i) The intersection  $H(\sigma) \cap A^+$  contains a vertical segment  $\tau$  that is to the right of  $W_0^s(p^+)$  and disjoint from  $U^+$ .
  - (ii)  $H(\sigma) \cap A^-$  contains a vertical segment  $\tau$  to the right of  $W_0^s(p^+)$  and disjoint from  $U$ .

**Remark 1** *In (H5), there is a slight change in the condition in comparison to the corresponding condition in [11]: originally, (H5) was about two-dimensional “vertical strips”, while in the above condition we only considered one-dimensional vertical segments. Notice that our (H5) is stronger, since every “vertical strip” contains a vertical segment.*

## B.2 Proof of conditions (H1)–(H5)

We now verify conditions (H1)–(H5). Most of the arguments are adapted from those in [11], while paying attention to the different form of the map  $H$ .

**Proof of (H1)–(H2)** Since the proofs of (H1) and (H2) are very similar, we will only prove (H1) here.

First, we investigate the position of  $H(\mathcal{R})$  projected onto  $(x, y)$ -plane. The image is given by

$$\{(y, \mu + y^2 + \beta x) \mid -4 \leq x \leq 4 \text{ and } -4 \leq y \leq 4\}.$$

Paying attention to the fact that the subset with  $x = 0$  is a parabola and the whole region is obtained via parallel displacement by  $\beta x$ , one can check that the intersection of this region with the square  $\{(x, y) \mid -4 \leq x \leq 4 \text{ and } -4 \leq y \leq 4\}$  has exactly two connected components. We denote the one in  $\{x > 0\}$  by  $A_0^+$  and the other one by  $A_0^-$ .

By a direct calculation, we can check that  $A_0^+ \subset \{(x, y) \mid 2.2 < x < 3.8\}$  and  $A_0^- \subset \{(x, y) \mid -3.8 < x < -2.2\}$ ; these properties are used repeatedly throughout this section. Observe that, therefore,  $H(\mathcal{R})$  is disjoint from  $\partial^s \mathcal{R}$ . Furthermore, notice that the end points of the parabola correspond to the projection of  $H(\partial^{uu} \mathcal{R})$  onto the  $(x, y)$ -plane, so that  $H(\partial^{uu} \mathcal{R})$  does not intersect  $\mathcal{R}$  or  $\mathcal{R} \cap H(\mathcal{R})$ .

Let us examine the configuration of  $H(\mathcal{R})$  in  $(x, y, z)$ -space. The points in  $H(\mathcal{R})$  are of the form  $(y, \mu + y^2 + \beta x, \xi z + y)$ . Thus, the set of points that project to a point in the  $(x, y)$ -plane forms a segment in  $(x, y, z)$ -space. Therefore, we can see that  $\mathcal{R} \cap H(\mathcal{R})$  has exactly two connected components; namely, one projecting to  $A_0^+$  and one projecting to  $A_0^-$ , which we denote by  $A^+$  and  $A^-$ , respectively. The component  $A^+$  is the candidate component satisfying condition (H1).

The non-emptiness of each of the components can be checked by calculating the  $z$ -coordinate directly; note also that  $p^+$  is contained in  $A^+$ . Moreover, the image  $H(\mathcal{R})$  ‘overflows’  $\mathcal{R}$  in the  $z$ -direction near the component  $A^+$  that maps to  $A_0^+$ . Indeed, the value  $\xi z + y$  is positive when  $z = 0$ , since only the part in  $\mathcal{R}$  with  $y > 0$  will map to  $A^+$ . Furthermore, if  $z = -40$ , then  $\xi z + y < -40$  for all  $-4 \leq y \leq 4$ , since  $\xi = 1.185$ . Hence, we can see that  $A^+$  is disjoint from  $H(\partial^u \mathcal{R})$  and the proof is complete.  $\square$

For the proof of condition (H3) we need to check several inequalities.

**Condition (H3)(i)** This condition claims two properties: the strict invariance of the cone field  $C^u$  and the uniform expansion of the vectors.

First, we check the strict invariance. Let  $p = (x, y, z) \in H^{-1}(A^+ \cup A^-)$  and recall that we have  $2.2 < |y| < 3.8$ . Take  $v = (s, t, u) \in \mathcal{C}^u(p) \setminus \{(0, 0, 0)\}$ . By definition, we have  $2|s| \leq \sqrt{t^2 + u^2}$ .

We denote the Jacobian matrix of  $H$  evaluated at  $p$  by  $D_p H$ . By a direct calculation, we can see that

$$D_p H = \begin{pmatrix} 0 & 1 & 0 \\ \beta & 2y & 0 \\ 0 & 1 & \xi \end{pmatrix}.$$

Moreover, we can see that  $D_p H(v) = (t, \beta s + 2yt, t + \xi u)$ . Hence, we need to check the inequality

$$2|t| < \sqrt{(\beta s + 2yt)^2 + (t + \xi u)^2}, \quad (9)$$

subject to the condition  $2|s| \leq \sqrt{t^2 + u^2}$  and  $(s, t, u) \neq (0, 0, 0)$ .

First, for  $s = 0$  inequality (9) is easily verified since  $4t^2 \leq 4y^2t^2$ . We now assume  $s \neq 0$  and let  $T = t/s$  and  $U = u/s$ . Then the inequality (9) is equivalent to

$$P(T, U) := (\beta + 2yT)^2 + (T + \xi U)^2 - 4T^2 > 0$$

subject to the condition  $4 \leq T^2 + U^2$ . By calculating the Hessian and the coordinates of the stationary point, we can see that  $P$  is a quadratic function that attains its unique minimum value inside the disk  $T^2 + U^2 < 4$ . Thus, if we confirm  $P(T, U) > 0$  on the circle  $T^2 + U^2 = 4$ , then  $P(T, U) \geq 0$  for  $T^2 + U^2 > 4$  as well.

We examine the function  $P(T, U)$  under the constraint  $T^2 + U^2 = 4$ . In the following, we assume  $y > 0$ , since the case  $y < 0$  can be covered by changing the variables  $(T, U) \rightarrow (-T, -U)$ . First, if  $(\beta + 2yT)^2 - 4T^2 \geq 0$  then we can easily see  $P \geq 0$ . Therefore, assume this is not the case, which happens when  $-\beta/(2y - 2) \leq T \leq -\beta/(2y + 2)$ . Since  $\beta = 0.1$  and  $2.2 < y < 3.8$  we only need to check the sign of  $P(T, U)$  for, say,  $-0.05 < T < 0$ . In this case the positivity of  $P$  is straightforward. Hence, the proof of the strict invariance is complete.

Let us check the uniform expansion of the vectors in  $\mathcal{C}^u$ . Assume  $v \in \mathcal{C}^u$ . Since  $\mathcal{C}^u$  is invariant, we have  $D_p H(v) \in \mathcal{C}^u$  as well. We want to compare the length of the vectors  $v$  and  $D_p H(v)$  with respect to the norm  $\|\cdot\|_0$ . That is, we need to check the inequality

$$t^2 + u^2 < (\beta s + 2yt)^2 + (t + \xi u)^2, \quad (10)$$

subject to the condition  $4s^2 \leq t^2 + u^2$ . Again, the proof of the case  $s = 0$  is straightforward, thus, we assume  $s \neq 0$ . We introduce the variables  $T$  and  $U$  as before, so that (10) is equivalent to

$$Q(T, U) = (\beta + 2yT)^2 + (T + \xi U)^2 - (T^2 + U^2) > 0, \quad (11)$$

subject to the condition  $T^2 + U^2 \geq 4$ .

Again, by calculating the Hessian and the coordinate of the stationary point, we can see that  $Q$  attains its unique minimum value at a point inside the disk  $T^2 + U^2 < 4$ . Therefore, we only need to check the positivity of  $Q$  on the circle  $T^2 + U^2 = 4$ . On this circle, notice that  $Q$  coincides with the function

$$Q(T, U) |_{T^2+U^2=4} = (\beta + 2yT)^2 + (T + \xi U)^2 - 4.$$

In the following, we assume  $y > 0$ ; the case  $y < 0$  can be deduced by changing the variables  $(T, U) \rightarrow (-T, -U)$ , as before. Furthermore, note that  $Q(T, U) \leq Q(-T, -U)$  if  $T \leq 0$ , so that we only need to consider the case  $T \leq 0$ .

If  $(T + \xi U)^2 - 4 > 0$ , then  $Q$  is positive. Therefore, assume  $(T + \xi U)^2 - 4 \leq 0$ .

By a direct calculation, we can see that this happens when  $U = \sqrt{(4 - T^2)} \geq 0$  and

$$-2 \leq T \leq 2 \frac{1 - \xi^2}{1 + \xi^2} \quad (12)$$

(so in the following we assume  $U \geq 0$ ).

Also, if  $(\beta + 2yT)^2 - 4 > 0$  then  $Q$  is positive, so we assume  $T > -\frac{2+\beta}{2y}$ . Hence, by combining with (12), we assume  $-\frac{2+\beta}{2y} < T < 2 \frac{1-\xi^2}{1+\xi^2}$ . Depending on the value of  $y$ , this case may be empty, in which case, the proof is already done. By a direct calculation, we have for  $\xi = 1.185$  that

$$-0.3363 < 2 \frac{1 - \xi^2}{1 + \xi^2} < -0.3362,$$

and, since  $\beta = 0.1$  and  $2.2 < |y| < 3.8$ , we have

$$-0.4773 < -\frac{2 + \beta}{2y} < -0.2763.$$

We assume that  $y$  is such that the interval is not empty. In this range, the following holds:

- The term  $(\beta + 2yT)^2$  is monotone decreasing as  $T$  increases (since  $-\beta/2y > 2\frac{1-\xi^2}{1+\xi^2}$  is almost equal to zero). Hence, we have

$$(\beta + 2yT)^2 \geq \left( \beta + 2y \cdot 2\frac{1-\xi^2}{1+\xi^2} \right)^2 > 1.9024.$$

- The term  $(T + \xi U)^2 = \left( T + \xi\sqrt{4 - T^2} \right)^2$  is monotone increasing as  $T$  increases, because  $\xi > 1$ . Therefore, we have

$$(T + \xi U)^2 \geq \left( -0.4773 + \xi\sqrt{4 - (-0.4773)^2} \right)^2 > 3.3277,$$

so that

$$Q(T, U) > 1.9024 + 3.3277 - 4 \geq 0,$$

on  $T^2 + U^2 = 4$  with  $U \geq 0$  and  $-\frac{2+\beta}{2y} < T < 2\frac{1-\xi^2}{1+\xi^2}$ . Hence,  $Q(T, U) \geq 0$  for all  $T^2 + U^2 \geq 4$  and we have the uniform expansion of the vectors.  $\square$

**Condition (H3)(ii)** By definition,  $\mathcal{C}^{uu} \subset \mathcal{C}^u$ , so (H3)(i) already implies uniform expansion of the vectors in  $\mathcal{C}^{uu}$ . We now investigate the forward invariance of  $\mathcal{C}^{uu}$ .

As before, we take  $p \in H^{-1}(A \cup A^-)$  and  $v = (s, t, u) \in \mathcal{C}^{uu}(p) \setminus \{(0, 0, 0)\}$ . Then, we have  $D_p H(v) = (t, \beta s + 2yt, t + \xi u)$ . To confirm that  $D_p H(v) \in \text{int}(\mathcal{C}^{uu})$ , we need to check

$$2\sqrt{t^2 + (t + \xi u)^2} < |\beta s + 2yt|, \quad (13)$$

subject to the condition  $2\sqrt{s^2 + u^2} \leq |t|$ , where  $(s, t, u) \neq (0, 0, 0)$ . Hence, we have  $|s| \leq |t|/2$  and  $|u| \leq |t|/2$ . Then the following estimates hold:

$$2\sqrt{t^2 + (t + \xi u)^2} \leq \left( 2\sqrt{1 + (1 + \xi/2)^2} \right) |t| < 3.7609 |t|$$

and

$$|\beta s + 2yt| \geq \left( 2|y| - \frac{\beta}{2} \right) |t| > 4.35 |t|.$$

Thus, we have the inequality (13).  $\square$

**Condition (H3)(iii)** The proof of (H3)(iii) is similar to the proofs of (H3)(i) and (H3)(ii), except that we work with the inverse map

$$H^{-1}(x, y, z) = \left( \frac{1}{\beta}[-x^2 + y - \mu], x, \frac{1}{\xi}[-x + z] \right).$$

Accordingly, we have

$$D_p H^{-1} = \begin{pmatrix} -\frac{2x}{\beta} & \frac{1}{\beta} & 0 \\ 1 & 0 & 0 \\ -\frac{1}{\xi} & 0 & \frac{1}{\xi} \end{pmatrix}.$$

We take  $p \in A^+ \cup A^-$  and  $v = (s, t, u) \in \mathcal{C}^s(p) \setminus \{(0, 0, 0)\}$ . First, let us check the backward invariance of  $\mathcal{C}^s$ . By a direct calculation, we have

$$D_p H^{-1} = \left( \frac{1}{\beta}[-2xs + t], s, -\frac{1}{\xi}[s - u] \right).$$

Therefore, for the invariance we need to prove the inequality

$$4 \left( s^2 + \frac{1}{\xi^2} (s - u)^2 \right) < \frac{1}{\beta^2} (-2xs + t)^2 \quad (14)$$

subject to the condition  $4(t^2 + u^2) \leq s^2$ , where  $(s, t, u) \neq (0, 0, 0)$ .

First note that we have  $|t| \leq |s|/2$ , so that we have

$$\frac{1}{\beta} |-2xs + t| \geq \frac{1}{\beta} (|2xs| - |t|) \geq \frac{1}{\beta} \left( |2xs| - \frac{|s|}{2} \right) \geq \frac{1}{\beta} \left( |2x| - \frac{1}{2} \right) |s| > 43.5 |s|.$$

In this estimate, we used the fact that  $2.2 < |x| < 3.8$  for  $p \in A^+ \cup A^-$ .

Similarly, we have  $|u| \leq |s|/2$ , which yields

$$\frac{1}{\xi} |s - u| \leq \frac{1}{\xi} \left( |s| + \frac{|s|}{2} \right) < 1.266 |s|.$$

These estimates imply inequality (14).

Let us now examine the uniform expansion of  $v$  with respect to the norm  $\|\cdot\|_0$ . Since both  $v$  and  $D_p H^{-1}(v)$  belong to  $\mathcal{C}^s$ , what we need to prove is

$$|s| < \frac{1}{\beta} |-2xs + t|,$$

subject to the condition  $4(t^2 + u^2) \leq s^2$ , where  $(s, t, u) \neq (0, 0, 0)$ . The argument is quite straightforward (using the inequality  $|s|/2 \geq |t|$ ) and omitted here.

This finishes the proof of (H3)(iii).  $\square$

For later use we present another property of  $H$  in the stable direction. We define another cone field,

$$\mathcal{D}^s(p) := \left\{ (s, t, u) \mid 20\sqrt{t^2 + u^2} \leq |s| \right\},$$

which is ‘thinner’ than  $\mathcal{C}^s$ . We have the following:

**Lemma 1** *The cone field  $\mathcal{D}^s$  is strictly backward invariant. More precisely, for every  $p = (x, y, z) \in A^+ \cup A^-$  and for every  $v \in \mathcal{D}^s(p) \setminus \{(0, 0, 0)\}$ , we have  $D_p H^{-1}(v) \in \text{int}(\mathcal{D}^s(H^{-1}(p)))$ .*

Lemma 1 holds if the inequality

$$400 \left( s^2 + \frac{1}{\xi^2} (s - u)^2 \right) \leq \frac{1}{\beta^2} (-2xs + t)^2$$

subject to the condition  $400(t^2 + u^2) \leq s^2$ , where  $(s, t, u) \neq (0, 0, 0)$ . Since the proof can be performed with a similar argument as for the invariance of  $\mathcal{C}^s$ , we again omit the proof.

**Proof of (H4)** To obtain condition (H4) we need to investigate the position of  $W_0^s(p^+)$ . Recall that  $p^+ = (x^+, y^+, z^+) \in A^+$ , with  $x^+ = y^+ = z^+(1 - \xi)$ , and  $3.565 < x^+ < 3.566$ . Since  $\xi = 1.185$ , we also have  $-14.405 < z^+ < -14.404$ . An important consequence of Lemma 1 is that we can localize the region where  $W_0^s(p^+)$  passes: Lemma 1 implies that  $W_0^s(p^+)$  is tangent to  $\mathcal{D}^s$ , so that the total variation of the  $(y, z)$ -coordinates along  $W_0^s(p^+)$  cannot exceed  $8/20 = 0.4$ . Together with the fact that  $W_0^s(p^+)$  contains  $p^+$ , we must have that  $W_0^s(p^+)$  is contained in the region

$$\{(x, y, z) \mid -4 \leq x \leq 4, 3.165 \leq y \leq 3.965, -14.805 < z \leq -14.004\}.$$

Now we are ready to examine condition (H4). Suppose that  $\sigma$  is a vertical segment to the right of  $W_0^s(p^+)$ . Since  $\sigma$  is tangent to  $\mathcal{C}^{uu}$ , the total variation of the  $z$ -coordinate cannot exceed  $8/2 = 4$ . Also, since  $\sigma$  is to the right of  $W_0^s(p^+)$ , none of the points in  $\sigma$  can have a  $z$ -coordinate smaller than  $-20$ . In particular, this means that every vertical segment to the right of  $W_0^s(p^+)$  must be contained in the region  $\{z \geq -20\}$ . Hence, by taking  $U^- \supset \partial^{u-}\mathcal{R}$  sufficiently small, no vertical segment to the right of  $W_0^s(p^+)$  will intersect  $U^-$ .  $\square$

**Proof of (H5)** Finally, we need to check condition (H5). As in [11], we just give an outline of the proof.

First, we choose two regions

$$\tilde{A}^+ := \{(x, y, z) \in \mathcal{R} \mid -4 \leq x \leq 4, 3.16 \leq y \leq 3.97, -19 \leq z \leq -5\},$$

$$\tilde{A}^- := \{(x, y, z) \in \mathcal{R} \mid -4 \leq x \leq 4, -3.8 \leq y \leq -2.2, -10 \leq z \leq 0\}.$$

Then, we define the notion of vertical segments in  $\tilde{A}^+$  and  $\tilde{A}^-$  in natural ways. Let  $\sigma$  be a vertical segment of  $\mathcal{R}$ . Using the fact that  $\sigma$  is tangent to  $\mathcal{C}^{uu}$ , that is, the total variation of its  $z$ -coordinate does not exceed 4, one can check that every vertical segment of  $\mathcal{R}$  to the right of  $W_0^s(p^+)$  contains a vertical segment of either  $\tilde{A}^+$  or  $\tilde{A}^-$ . We denote such a segment by  $\sigma'$ . Then, by a direct calculation, one can check that  $H(\sigma')$  contains a vertical segment of  $\mathcal{R}$  to the right of  $W_0^s(p^+)$ : if  $\sigma' \subset \tilde{A}^-$ , this is obvious. If  $\sigma' \subset \tilde{A}^+$  then using  $\sigma' \subset \sigma$  and investigating the behaviour of  $H$  in the  $z$ -coordinate, we can see that  $H(\sigma') \cap \mathcal{R}$  is to the right of  $W_0^s(p^+)$ .

Thus, in either case, we observed that we can take the segment as claimed.  $\square$

## References

- [1] A. BACK, J. GUCKENHEIMER, M. MYERS, F. WICKLIN, AND P. WORFOLK, *DsTool: Computer assisted exploration of dynamical systems*, Notices Amer. Math. Soc., 39 (1992), pp. 303–309.
- [2] R. BAMÓN, J. KIWI, AND J. RIVERA-LETELIER, *Wild Lorenz-like attractors*. arXiv 0508045, 2006. Available at <http://arxiv.org/abs/math/0508045>.
- [3] M. BENEDICKS AND L. CARLESON, *The dynamics of the Hénon map*, Ann. of Math. (2), 133 (1991), pp. 73–169.
- [4] C. BONATTI, S. CROVISIER, L. J. DÍAZ, AND A. WILKINSON, *What is... a blender?*, Notices Amer. Math. Soc., 63 (2016), pp. 1175–1178.
- [5] C. BONATTI AND L. J. DÍAZ, *Persistent nonhyperbolic transitive diffeomorphisms*, Ann. of Math. (2), 143 (1996), pp. 357–396.
- [6] C. BONATTI AND L. J. DÍAZ, *Abundance of  $C^1$ -robust homoclinic tangencies*, Trans. Amer. Math. Soc., 364 (2012), pp. 5111–5148.
- [7] C. BONATTI, L. J. DÍAZ, AND S. KIRIKI, *Stabilization of heterodimensional cycles*, Nonlinearity, 25 (2012), pp. 931–960.
- [8] C. BONATTI, L. J. DÍAZ, AND M. VIANA, *Dynamics beyond Uniform Hyperbolicity. A global geometric and probabilistic perspective*, vol. 102 of Encyclopaedia Math. Sci., Springer-Verlag, Berlin, 2005.

- [9] P. CVITANOVIĆ, *Periodic orbits as the skeleton of classical and quantum chaos*, Phys. D, 51 (1991), pp. 138–151. Nonlinear science: the next decade (Los Alamos, NM, 1990).
- [10] R. DEVANEY AND Z. NITECKI, *Shift automorphisms in the Hénon mapping*, Comm. Math. Phys., 67 (1979), pp. 137–146.
- [11] L. J. DÍAZ, S. KIRIKI, AND K. SHINOHARA, *Blenders in centre unstable Hénon-like families: with an application to heterodimensional bifurcations*, Nonlinearity, 27 (2014), pp. 353–378.
- [12] J. P. ENGLAND, B. KRAUSKOPF, AND H. M. OSINGA, *Computing one-dimensional stable manifolds and stable sets of planar maps without the inverse*, SIAM J. Appl. Dyn. Syst., 3 (2004), pp. 161–190.
- [13] S. V. GONCHENKO, I. I. OVSYANNIKOV, C. SIMÓ, AND D. TURAEV, *Three-dimensional Hénon-like maps and wild Lorenz-like attractors*, Internat. J. Bifur. Chaos Appl. Sci. Engrg., 15 (2005), pp. 3493–3508.
- [14] S. V. GONCHENKO, L. P. SHILNIKOV, AND D. V. TURAEV, *On global bifurcations in three-dimensional diffeomorphisms leading to wild Lorenz-like attractors*, Regul. Chaotic Dyn., 14 (2009), pp. 137–147.
- [15] M. HÉNON, *A two-dimensional mapping with a strange attractor*, Comm. Math. Phys., 50 (1976), pp. 69–77.
- [16] S. HITTMAYER, B. KRAUSKOPF, AND H. M. OSINGA, *Interacting global invariant sets in a planar map model of wild chaos*, SIAM J. Appl. Dyn. Syst., 12 (2013), pp. 1280–1329.
- [17] ———, *From wild lorenz-like to wild rovela-like dynamics*, Dynam. Syst., 30 (2015), pp. 525–542.
- [18] B. KRAUSKOPF AND H. OSINGA, *Investigating torus bifurcations in the forced Van der Pol oscillator*, in Numerical Methods for Bifurcation Problems and Large-Scale Dynamical Systems (Minneapolis, MN, 1997), vol. 119 of IMA Vol. Math. Appl., Springer-Verlag, New York, 2000, pp. 199–208.
- [19] B. KRAUSKOPF AND H. M. OSINGA, *Growing 1D and quasi-2D unstable manifolds of maps*, J. Comput. Phys., 146 (1998), pp. 404–419.
- [20] ———, *Computing geodesic level sets on global (un)stable manifolds of vector fields*, SIAM J. Appl. Dyn. Syst., 2 (2003), pp. 546–569.
- [21] D. LI, *Homoclinic bifurcations that give rise to heterodimensional cycles near a saddle-focus equilibrium*, Nonlinearity, 30 (2017), pp. 173–206.
- [22] E. LORENZ, *Deterministic nonperiodic flow*, J. Atmospheric Sci., 20 (1963), pp. 130–141.
- [23] G. MASON, A. HAMMERLINDL, B. KRAUSKOPF, AND H. M. OSINGA, *Exploring the neighbourhood of heterodimensional cycles*. In preparation, 2017.
- [24] C. G. MOREIRA, *There are no  $C^1$ -stable intersections of regular Cantor sets*, Acta Math., 206 (2011), pp. 311–323.
- [25] S. E. NEWHOUSE, *Nondensity of axiom A(a) on  $S^2$* , in Global Analysis, Proc. Sympos. Pure Math. XIV, Amer. Math. Soc., Providence, RI, 1970, pp. 191–202.

- [26] J. PALIS AND W. DE MELO, *Geometric Theory of Dynamical Systems*, Springer-Verlag, New York, 1982.
- [27] C. ROBINSON, *Dynamical Systems: Stability, Symbolic Dynamics, and Chaos*, Studies in Advanced Mathematics, CRC-Press, 1999.
- [28] M. SHUB, *What is ... a horseshoe?*, Notices Amer. Math. Soc., 52 (2005), pp. 516–517.
- [29] C. P. SIMON, *A 3-dimensional Abraham-Smale example*, Proc. Amer. Math. Soc., 34 (1972), pp. 629–630.
- [30] D. V. TURAEV AND L. P. SHILNIKOV, *An example of a wild strange attractor*, Mat. Sb., 189 (1998), pp. 291–314.
- [31] ———, *Pseudo-hyperbolicity and the problem on periodic perturbations of Lorenz-like attractors*, Russian Dokl. Math., 77 (2008), pp. 17–21.
- [32] R. URES, *The abundance of hyperbolicity in the  $C^1$  topology*, Ann. Sci. École Norm. Sup. (4), 28 (1995), pp. 747–760.
- [33] W. ZHANG, B. KRAUSKOPF, AND V. KIRK, *How to find a codimension-one heteroclinic cycle between two periodic orbits*, Discrete Contin. Dyn. Syst. Ser. A, 32 (2012), pp. 2825–2851.